Bio-ethylene production: from reaction kinetics to plant design

Antonio Tripodi, Mattia Belotti, Ilenia Rossetti*

Chemical Plants and Industrial Chemistry Group, Dip. Chimica, Università degli Studi di Milano, CNR-ISTM and ISTM Unit Milano-Università, via C. Golgi 19, 20133 Milano, Italy.

Abstract

Ethylene production from renewable bio-ethanol has been commercially proposed in recent years as a sustainable alternative to fossil sources. The possibility to exploit diluted bioethanol as less expensive feedstock was studied both experimentally, using different catalysts at lab-level, and through preliminary process designs. In this work a full-scale plant simulation is presented, built on a detailed reaction kinetics, based on literature data. Rate equations for the primary and side reactions are revised and implemented within the Aspen Plus® simulation package, using a range of thermodynamic methods, as best suited to the different process stages. The catalyst loading within the reactor can be effectively distributed according to the underlying kinetics and the overall plant layout lets foresee the best routes for the material recycles. The detailed reaction modeling and the choice of the thermodynamic models showed essential to obtain reliable predictions. Setting a target yield of 10^5 t/year of polymer-grade ethylene, the reactive section must be fed with 76 t/h of diluted ethanol and operated below 400 °C. The energy input amounts to 17 MW_{el} plus 73 MW_{th}. This newly designed process sets the sustainable ethylene production on a detailed and reassessed computational basis.

Keywords: Ethylene; Bioethanol; Olefins production; Kinetic modelling; Process design and simulation; Aspen Plus.

* Corresponding author: email: ilenia.rossetti@unimi.it; fax: +3901250314300

Introduction

Turning biomass into chemicals, besides using it as a fuel [1], is likely to be the actual way to rise its value over that of the fossil feedstock, notwithstanding the leap from non-renewable towards circular processes [2–4]. Among other molecules, bioethanol is particularly interesting as the starting point for a C2-based chemical platform, by itself [2,5–7] and also as a preferred precursor of ethylene [8–13], which is the basis for many further chemicals.

Given the well-established role of the latter compound as building block for a number of other important molecules (*e.g.* ethylene glycol, acetic acid) and materials (polyethylene and vinyl chloride derivatives) and spanning also the C3 and C4-based chemical platforms (due to the relative ease of ethylene dimerization), any improvement in the ethanol-to-ethylene process helps to expand the value of this alcohol and of its feedstock well beyond the traditional use as fuels [3,14].

Bioethanol production plants are an established technology [15–18], now available also from 2nd generation or mixed feedstock [19,20]. Several facilities worldwide provide a fully-integrated chain from bioethanol to polyethylene, where the actual ethylene production starts from concentrated ethanol solutions [21–23]. This choice is not necessarily the less expensive and is related to the fact that most bioethanol plants are optimized for a fuel-grade product (that has a higher market price), while the green-ethylene process can actually be operated with non-anhydrous ethanol through dehydration of the alcohol, which is catalyzed by acidic catalysts.

Former ethanol-to-ethylene plants used alumina for dehydration and crude ethylene was often sweetened by caustic wash [24,25]. The more expensive zeolites are instead chosen to dehydrate bioethanol at lower temperature [22,23,26]. Different plant data were reviewed as a starting point for process design [12,26–28]. According to these, the byproduct spectrum [29] was identified, and the target yield relevant for further optimization studies was fixed to 100 kton/year of ethylene, a scale in line with the up-to-date renewable processes [27].

On acidic catalysts, ethanol can lose a hydrogen atom turning into ethoxide or dimerize to diethyl ether (or dimerize with the ethoxide itself): ethylene is formed preferentially via ether breaking, less probably via direct C-O bond activation and ethanol dehydration, though this depends also on the particular catalyst [30–33]. The further dehydrogenation of the ethoxide into acetaldehyde, otherwise, leads eventually to acetic acid or to methane and carbon monoxide formation [34,35] – though the acetaldehyde can also mediate the ethylene re-hydrogenation into ethane without yielding C_1 byproducts [36,37]. Longer olefins start forming at high contact time after ethylene polymerization [38,39], and carbonaceous deposits grow on this basis though they are partially removed by the steam formed (or purposely co-fed) in the reaction mixture [37]. The role of water in the kinetic mechanism itself is less clear [31], though is generally considered an antagonist for ethanol adsorption [32] (the issue is shortly reviewed in [40]).

Currently, there is a yet unfilled gap between rather complex kinetic models derived by a-priori analysis and more compact formulations that interpolate heuristically many lab-derived data [41]. These latter, in turn, refer to reaction conditions of very high selectivity (*e.g.* [40,42], besides the references cited above), that do not always reproduce the actual outcome of plant reactors (where the different scale and the catalyst management lead to more byproducts).

On the other hand, full-plant calculation are nowadays available [9,22,29,43–45], aided by the availability of simulation software relatively easy to use, with wide databanks of thermodynamic properties. These studies aim essentially at the overall reassessment of the mass and energy balances in view of their economic optimization, and often resort to several simplifications:

- the reactor redistributes the ethanol moles into a product spectrum derived by plant or equilibrium data: in this way the kinetic effect of the reaction temperature is treated independently on a heuristic basis and it is not possible to ascertain the detailed effect of the catalyst load on the conversion;

- the separation section is based on one thermodynamic model only and the choice is not always supported by a survey of the property databanks.

Other simulation works based on more realistic kinetic reactors, instead, do not consider with sufficient detail and extension the other plant's sections [46,47].

In this paper, we propose an overall simulation of an ethanol-to-ethylene plant based on a reaction kinetic model derived from laboratory data, with the goal to link the microscopic to the ton-scale ends of the process. The separation section, in turn, is calculated after the reassessment of thermodynamic models with available data.

In this way, the relation between i) the reaction temperature, ii) the contact time and iii) the byproduct formation are directly connected by the chosen activation energies. The separation blocks are never treated as 'black boxes' that just route different chemicals to different streams, but are sensitive to the adopted temperatures and actual streams compositions. Thanks to this approach, the mass and energy balances are intrinsically connected and the detailed choice of a separation method or reactor arrangement have a directly appreciable effect. The general calculation becomes then more reliable and the key steps, with stronger impact on the results, are easier to detect.

Though the gas sweetening strategy is strongly dependent on the actual CO_2 quantity produced, an up-to-date amine washing treating is here presented, as an independent plant module that can be optimized also for syngas treatment in the general framework of multi-purpose biorefineries. Also the most convenient strategies for the feed concentration and steam addition are reassessed from the point of view of thermal integration: this opens the way to the use of bioethanol as a less expensive feedstock to improve the feasibility of this route to green ethylene.

Materials and methods

Modelling of reaction kinetics was carried out through home-developed Matlab® (MathWorks Inc.) scripts. The plant simulation was accomplished using the software Aspen Plus® v.8.0 and Aspen Adsorption® (Aspen Tech Inc.). The thermodynamic models used were: Non-Random Two-Liquids (NRTL, activity coefficient for liquid phase) coupled to the Redlich-Kwong equation of state (RK, for the vapor phase), Predictive-Redlich-Kwong-Soave (PSRK, equation of state model for both vapor and liquid phases) and Henry pressure-solubility correlation. The formulation and parametrization of these models for the listed chemicals (**Table 1** and **Table 2**) were already available within the used release of Aspen Plus®.

In addition, the Electrolytes-NRTL (ENRTL) model coupled with the Henry's law was used for the solubility of CO_2 in water, followed by the first dissociation of carbonic acid.

Ethanol dehydration kinetics

To set the reaction kinetics into a whole plant simulation, we limited our choice to simple Langmuir-Hinshelwood-Hougen-Watson (LHHW) formulations to account for the strong affinity of the acidic catalysts commonly employed to water and ethanol. While most laboratory data are treated with even simpler formulas, an adsorption term provides at least two advantages:

- it constitutes a conceptual link to the more detailed models derived from theoretical studies, some compared successfully to micro-scale data;
- provide a natural representation of the reactions slowing down without introducing empirically negative exponents for some partial pressures (usually for water).

The model used is based upon the following stoichiometry and is also reported in **Table 3** (the datum supplied refers to the reaction enthalpy):

$C_2H_6O \rightleftarrows C_2H_4 + H_2O$ 45 kJ/mol Direct ethanol dehydration (1)

$2\ C_2H_6O \rightleftarrows C_4H_{10}O + H_2O$	-12 kJ/mol	Ethanol dimerization	(2)
$C_2H_6O \rightleftarrows C_2H_4O + H_2$	184 kJ/mol	Ethanol dehydrogenation	(3)
$C_4H_{10}O \rightleftarrows 2\ C_2H_4 + H_2O$	115 kJ/mol	Diethyl-ether cracking	(4)
$2\ C_2H_4\ \rightleftarrows C_4H_6 + \ H_2$	-52 kJ/mol	Ethylene dimerization	(5)

The reaction enthalpies reported for each reaction are derived from [48].

The reaction rates are represented with the general formula (for the molar fractions *y* of every i-th species in the j-th reaction, where the dimensions are carried by the preexponential factor *k*°):

$$r_j = k^0{}_j \left(e^{-E_a/RT}\right) \frac{\prod_i y_i^{\alpha_{i,j}}}{\left(1 + \sum_n K_n \prod_i y_i^{\beta_{i,n}}\right)^{d_j}} \left[\frac{mol}{s \times g_{cat}}\right] \quad (6)$$

This model was used to interpreter the data by Kagyrmanova et al. [49], even if these authors opted for a different formulation, because the goal of the present work was anyway the simulation of reactions mixtures with a higher water content. The reactor molar and energy balances were then solved, at any point, under the assumption of an ideal plug-flow, without diffusion, according to the monodimensional equations:

$$\frac{\partial n_i}{\partial t} = -u\frac{\partial n_i}{\partial x} + \ w\sum_j \nu_{ij} r_j = 0 \quad (7)$$

$$\frac{\partial T}{\partial t} = -u\frac{\partial T}{\partial x} + \frac{w}{\bar{C}}\sum_j r_j \Delta H_j = 0 \quad (8)$$

(where *w* is the catalyst mass, *u* the reacting gas advection velocity, $\bar{C}$ the mixture molar heat capacity in the control volume and *H* its enthalpy). The coupled equations are integrated, for the steady state, over the reactor length *x* by an embedded routine. The above mentioned laboratory data were then retro-fitted adjusting the kinetic constants of the reaction rates, but keeping the activation energies fixed: a similar analysis was already carried out by Maia et al. [50], though a direct comparison of the

parameters cannot be done because these authors employed a non-isothermal model with diffusive corrections.

On the other hand, the reported stoichiometry was extended to consider possible byproducts coming from reforming-like parasitic reactions (also observed using acidic oxides [9,25,51]):

$C_2H_6O \rightleftarrows CO + CH_4 + H_2$	49.6 kJ/mol	Ethanol decomposition	(9)
$C_2H_6O + H_2O \rightleftarrows CO_2 + CH_4 + 2H_2$	8.49 kJ/mol	Ethanol decomposition + WGS	(10)

adjusting again the kinetic preexponential factors to comply with known data [25], but fixing the activation energies to the values obtained in [52]. At this stage, we choose to neglect the pressure correction, because we did not want to make assumptions on the catalyst particle dimensions and roughness. This has no impact, anyway, on the thermal exchanges calculation since we adopted the option of adiabatic reaction stages with dedicated inter-cooling sections [9,29,44,53].

Review of thermodynamic properties

The thermodynamic models taken into account (*vide supra*) were initially compared against the data reported in [54,55] and [56].

When the stream was totally in gas-phase, we adopted the PSRK EoS, because we found it more reliable to describe the binary equilibria ethanol-ethylene and water-ethylene. When a liquid phase was present, the NRTL description for the ternary mixture led to more conservative results in terms of ethanol solubility, so we switched to the mixed NRTL-RK approach (see **Figure 1** and **Figure 2**). Unfortunately, we could not find ternary equilibrium data for temperature ranges as low as foreseen in our first separator, nonetheless this choice is in line with other works [29,45].

The residual ethylene solubilized in the flash bottoms is described correctly only resorting to the Henry's constant approach (the parameters were retrieved by the AP databank for the ethylene-water pair, and derived from [57] for the ethylene-ethanol pair). In this case, the adoption of the NRTL-RK model was mandatory, because EoS methods do not allow the contemporary use of Henry constants (**Figure 2**) in Aspen Plus®.

The reviewed VLE data between ethylene and butylene [55] were reproduced fairly by a series of models, among which PSRK looks the finest (**Figure 3**).

Review of existing plant data

Some of the reviewed plant data are summarized in **Table 4**. Mono-carbon species are essentially a consequence of the residual presence of the ethanol reforming reactions: carbon dioxide is formed by the water-gas shift equilibrium arising when ethanol breaks, giving carbon monoxide and methane. Ethane is formed mostly by re-hydrogenation of the ethylene [36]. See also[29] and [44] for two typical byproduct spectra.

Plant sections and computing methodology

The plant flowsheet was organized and calculated as divided into different sections. This allowed to switch from one thermodynamic model to another according to the issues specified above and, moreover, to solve separately the recycle between the two amine-washing columns. Keeping the different methods under separate flowsheets avoids the occurrence of spurious thermal ins/outs. In general, routing into a block calculated with 'MOD2' a stream issued by a block under 'MOD1', it might be calculated a $\Delta H = \dot{m}\left[h_{MOD2}(T, P, x_j) - h_{MOD1}(T, P, x_j)\right]$ belonging to the second block's

balance (x_j are the specie fractions, $\dot{m}$ the mass flow). The relevant mass recycles where then linked into the respective sections according to the results (**Figure 4**).

Reactive section

The reactor was modeled into three adiabatic stages with the relative re-heaters. The recycled ethanol is fed after the first stage (see also **Figure 5** left), in order to boost its concentration after a part of it has been converted. The initial feed heating is carried out partly by cooling the reaction products, and then via a hot utility. The temperature range chosen is the suggested one for the Alumina-based catalysts (*ca.* 400 °C), then every pre-heating brings the process gas to 430 °C to overcome the cooldown due to the reaction endothermal behavior.

Primary separation

This section is composed of a flash separator that recovers the ethylene vapor, while most of the water (together with unreacted ethanol and the polar byproducts) is discharged with the bottom liquid. An ethanol recovery column is then placed right upstream the reactor recycle. This configuration actually shifts the point of the ethanol purification within the whole bioethanol-to-ethylene process, allowing to reduce the number of process blocks (see **Figure 5** and **Figure 6**).

Other layouts foresee a separated steam-injection section upstream the reactor (after the column that pre-concentrate the alcohol) and a recovery column in case the catalyst does not grant a 100% conversion; our choice can be as flexible (the ethylene reactor is still an independent module that can be added alongside a standard fuel-grade ethanol production, but *in parallel* to the final alcohol purification rather than after it), and reaches a higher level of integration between plant sections. Feeding azeotropic ethanol into the reactor means to rely on the generated water only to remove the carbonaceous deposits from the catalyst.

The alcohol recovery column is not specified to achieve a good purity, and the reflux ratio is maintained by the reboiler only, thanks to the condensation performed upstream.

The reactor feed and product stream crosses in the regenerative heat exchanger H106 (**Figure 6** left), that substantially reduces the overall energy input of these two first plant sections (see also the plant and block reports).

Secondary separation

In this section, most of the water vapor is condensed by four pressurization stages (**Figure 6** right) with a constant ratio of 2.0. A 4-stage compression represented a good compromise to evaluate the temperature/duty cascade of a multi-stage process (that gains efficiency) without using a too complicated flowsheet nor, on the other hand, leaving the details within a multi-stage compressor that is treated by Aspen Plus® as a black-box.

In this calculation, the compressors were considered as ideal. Between each compression the gas was cooled down to 20 °C, this value was selected as the lowest temperature that can be handled with air or water as cooling utilities. The trade-off between the compression and the cooling duties will be analyzed in further developments, together with the efficiency of these units for economic assessment.

CO_2 removal through amine scrubbing

A CO_2 sweetening unit is needed to comply with a polymer grade purity. For this reason, all the ethanol-to-ethylene plants (since the 60s), and all the reviewed simulation works feature a CO_2 removal section (though not necessarily an amine-based one). The separated CO_2 is intended for storage and, possibly, selling.

Unlike other gases, carbon dioxide can be effectively removed by scrubbing with bases due to its acidic character. While some processes [12,23–25] and, as a consequence, also simulation works [46] foresee alkaline solutions circulating between an adsorbing and stripping column, in this work it is included an amine-based CO_2 capture system. This choice has lately become the standard for the sweetening of large gas flows [58], because it can sensibly speed-up the absorption of CO_2 into water while decreasing the issue of solid salt formations with respect to older processes [59,60]. Moreover, the

pressure increase usually needed to enhance CO_2-water solubility is already performed in the upstream condensation section.

From the computational point of view, however, this choice introduces two rigorously modelled distillation columns connected between themselves within a mass and energy loop (**Figure 7**), which constitutes a major increase in the simulation's complexity. In this case, the thermodynamic model chosen was the ENRTL-RK, which can represent the mixture properties in presence of known charged species, once the reactions that define their balances are known (**Table 6**). We adopted four simplifications:

- the columns stages are in equilibrium, with an efficiency of 100%;
- the charged species are always in simultaneous equilibrium;
- only the bicarbonate anion is present;
- we used as basic species the N-Methyldiethanolamine (MDA) without a further review of its already provided thermodynamic parameters.

Final ethylene dehydration

The amine-washing recycle causes a little increase of the gas humidity: to remove the residual water, here we considered a pressure-swing adsorption (PSA) on zeolites, since this option does not require heat inputs and can take advantage of the already achieved overpressure. Another option is proposed by Becerra et al. [43], but more complex both from the technological and chemical point of view.

Unlike assumptions made in other papers, that do not consider the specific dehydration method [9,22,29,45,46], or foresee the PSA strategy as a once-through train in series [44], the section adds another recycle loop. This choice is based upon the fact that if the adsorption beds are regenerated via a third gas (*e.g.* nitrogen [44]), a little part of the process gas should be used to carry away also the inert content trapped within the solid, while using a fraction of the dry ethylene as the purge stream there is no

need of additional pressurized gas lines. This approach is also common for similar ethanol dehydration layouts [61,62].

As a preliminary calculation, very conservative requirements of pressure difference (from 5 to 1 bar) and water initial content (2% molar) were considered, leading to a recycled humid gas of 22 ton/h against a nominal plant size of 45 ton/h of dry ethylene. The recycle stream is recompressed and cooled to enter the CO_2 absorbing column at the same condition (15 atm, 20 °C) of the main stream coming from section 2.

The layout of a two-bed, 4-step cycle PSA system is represented in **Figure 8**. In steady operation, the average composition of the main outflow (stream 501) and of the recycle (stream 302) are constant.

Olefin separation

On acidic catalysts, ethylene itself can form unsaturated dimers (butane, butylene), as revealed either by laboratory and plant data. Lab-scale studies on dehydration are usually performed in high selectivity conditions, so C4 olefins are a minor byproduct. Nevertheless changing the reaction conditions the ethylene polymerization into C4, C6 and heavier products (even aromatics) can be obtained [63].

All the reviewed plant layouts, therefore, foresee a final separation train at cryogenic temperatures, whose details depend on the target ethylene purity, the residual non-condensable gases and the adopted pressure. Taking butylene as the most important heavier byproduct, its separation can be achieved with a single cryogenic column. It was chosen to work at the same pressure of the PSA section (5 atm), the trade-off between a higher pressure option and a compression-expansion layout will be considered in the future.

The scheme in **Figure 9** reports also the simpler solution to provide a cryogenic heat sink, which uses the purified ethylene itself.

Results

Reactor output

The data from the experimental study by Kagirmanova et al. [49] under isothermal conditions were reproduced first, in order to check the coherence of the new kinetic model (**Figure 10**). Then, to align the virtual reactor outcomes to the calculation of Maia et al. [50], the kinetic constants were re-optimized imposing the same temperature profile calculated by these latter (same figure – notice also that a similar shape of the temperature profile in lab-scale tests on alumina was reported independently in [64]). This adjustment was necessary, because a plug-flow reactor model in Aspen Plus® does not consider the diffusion and thermal gradients calculated in the cited literature. Afterwards, the side-reactions constants were tuned, so to yield a spectrum of by-products in line what the data already reviewed.

Notice that, with the adopted model, butene sensibly increases its production rate when there is enough ethylene present, so that an acceptable selectivity to ethylene can be maintained only if there is always some ethanol present (**Figure 11**). This behavior suggests to limit the ethanol conversion below 100% and to recycle the unreacted ethanol, even if it leads to a build-up of the heavier species concentration. Bringing the alcohol to full conversion without recycles could lead to a parallel increase of butene at the expenses of the ethylene.

The similar and linear shape of the adiabatic thermal profile (**Figure 12** left) through the three stages is due to the fact the heat adsorption is determined by the water formation and the C_2 conversion rate follows linearly the conversion of ethanol, as acetaldehyde and C_1 byproducts are negligible from this point of view. The results shown were obtained loading three adiabatic reaction stages with 70, 80 and 80 kg of catalyst each, so that the overall contact time refereed to the ethanol fed only was *ca.* 13 s (GHSV = 330 h^{-1}). This value has been selected after a preliminary screening of the reaction

conditions and represented a reasonable compromise between conversion, selectivity, temperature profile in the reactor and consequent duties.

Despite the process is globally endothermal, the foreseen reheating strategy maintains a slight increase of the average temperature of each stage (**Figure 12** right), and the continuous conversion of diethyl ether into ethylene maintains the selectivity (calculated on ethanol consumption basis) steadily above 60% mol/mol.

At last, it should be underlined that for a reliable sizing of the reactor a reliable effectiveness factor is needed. However, at this stage we have considered it as unit since the correct computation of the effectiveness factor should be based on the knowledge of the effective diffusivity, in turn calculated based on the porosity and tortuosity factors. At the moment insufficient data on the catalyst used in the adopted literature is available.

Primary separation and reactor recycle

The key specifications and results for the flash separators and the recovery column are reported in **Table 5** and in **Figure 13** respectively. Also a single-block layout was tested, *e.g.* a column with a partial condenser, but to achieve similar performances in terms of ethanol recovery and ethylene separation, a roughly double heat input was calculated at the reboiler, so this option was discarded. The flash separation block was kept at 40 °C, because this value is large enough to employ standard cold utilities and to keep water and ethanol within a 10% mol/mol respect to the ethylene flow.

The mass balance of the reactive and first separation sections can be traced in **Figure 14**: the reactor path is not much influenced by the recycle of the column vapor distillate. Taking the flash vapor as depending only on its pressure and temperature, the column balances can be adjusted to obtain always a full ethanol recovery.

In this first overall simulation, a detailed energy optimization was not attempted, yet two regenerative exchanges were foreseen: from the cooling reaction mixture to the reboiler of the recovery column, and furtherly to the feed. A total of 84-85 MW can be kept in this way within the reactor, roughly 70 via the regenerative heat exchanger. The preliminary design was performed (see also **Figure 15**) with a pinch point of 5 °C only, because of the contact of a condensing vapor and a boiling fluid. We must point out that this block is crucial, not only for the energetic economization (its duty is the 43% of all the unit operations before the first flash separator), but also because the feasibility of the heat transfer is due to a calculated dew-point in the hot fluid higher than the boiling point of the hydro-alcoholic feed, so the reliability of the thermodynamic models is fundamental.

The heat input of the production section in charge of the hot utilities is calculated as 72 MW circa, 50 to vaporize and heat the feed up to 430 °C and 22 MW to cope with the globally endothermic reactions. Notice that feeding the same quantity of ethanol at azeotropic purity would require just 40 MW for the heating and only 14 MW for the cooling: of these latter, approximately 75% are likely to be recoverable, making an approximate calculation over the temperature cascade, leaving 30 MW to the hot utility. This value is comparable with the 50 MW foreseen in presence of large water quantities and, moreover, leaves out the duty of the ethanol concentration column. Also the processes referenced above consider to feed both ethanol and water into the reactor.

The issue about ethanol purification is then shifted upstream: other organic molecules produced together with ethanol in bio-refineries must be kept within the catalyst tolerance, and their amount is related to the ethanol concentration achieved in the rectification columns, beyond the pre-concentration stages [37,65,66].

The first and second sections together yield 99.8% (on molar basis) of the fed ethanol as ethylene, the heat input is 1.08 kW per kg/h of ethylene and the heat released to cold utilities 0.83 kW per kg/h of ethylene.

Water condensation

The main separation of the water vapor is achieved by a train of 4 compression stages with intercooling and condensate discharge. This solution has the advantage of being technologically simple and robust and at the high water fractions of this section, more sophisticated systems are not needed. The layout derives from different compromises:

- while more stages decrease the power consumption (keeping the gas at lower temperatures), they increase the simulation complexity;
- reaching a pressure of 16 atm, the final water fraction in the vapor is 0.036 % mol/mol, so further stages or pressure increases are not useful (according to the calculation of the NRTL-RK model), the corresponding fraction of ethanol is about double, while diethyl ether is the 0.3 % mol/mol.

Notice that, anyway, these fractions increase substantially if the Henry constant or the PSRK EoS are used (water: 0.12 % and 0.15 % mol/mol, ethanol: 0.34 % and 0.30 % respectively). We discarded the Henry constants because all the parameters surveyed were originally retrieved in conditions too different from the simulated one and we kept the NRTL description of the liquid phase as more reliable with respect to ethanol.

As expected, most of the heat release is determined by the first cooler-separator couple (47 % of the total), due to a calculated Δh of 247 kJ/kg averaged on the whole stream. This section recovers 97.7% of the ethylene, requires 4700 kW_{el} (0.104 every kg/h of ethylene) and has to discharge 7580 kW_{th} (0.17 on the same ethylene basis) to the cold utilities.

CO_2 removal

The gas sweetening section was designed to treat the compressed ethylene stream, together with the recycled purge stream of the downstream dehydration. At atmospheric pressure, in fact, the CO_2 solubility in the aqueous amine solution would be too low (while a high partial pressure is needed to enhance the catalytic role of the amines in the capture kinetic [60]), and keeping the recycle pressurization in parallel to the main train could help to limit the maximum size of the compression units.

The washing solution helps to furtherly remove the condensable impurities from the ethylene stream (21 ppm left), while the equilibrium calculation foresees a CO_2 quantity of 86 ppb. Considering to perform the downstream dehydration on adsorbing solids, the residues of ethanol and diethyl ether are likely to be treated together with water (2400 ppm) on the very acidic materials commonly employed in these techniques (see for example [67] for a parallel treatment of polar from a non-polar carrier), the following section can then be sized for 3000 ppm of impurities.

The MDA loading in the absorption-regeneration cycle is about 10 times (on a molar basis) the CO_2 fed (0.1 kmol/h), this quantity is required to effectively push the adsorption equilibrium to the right as H_2CO_3 is a weak acid, and is in line with other literature values [68]. The reflux ratio in the CO_2 stripper (4 mol/mol) is also determined by the excess of water calculated to shift again the carbonic acid equilibrium to the left. The partial condenser is specified to work at the calculated dew point (88 °C), in order to let out all the CO_2 overhead. The quantity of other substances showing an appreciable vapor pressure at this temperature is not important, then the second stripper specification is to produce 9% of the feed as vapor distillate.

This helps the column calculation to align itself to the recycle stream variations in the convergence steps. The simulation of this section was more difficult than any of the other, due to the contemporary presence, within the same recycle loop of:

- six additional chemical species (MDA, $MDAH^+$, HCO_3^-, H_2CO_3, OH^-, H_3O^+): the carbonate anion was neglected because it overloads the calculation but it is not as relevant as the other specie at pH<10 [59] (see **Table 6** and **Figure 16** for details);
- algebraic bounds between the electrolytes, coming from the equilibrium chemistry, to be satisfied independently;
- a rigorous column with two degrees of freedom (the adsorbing column suffered convergence issues only at too low fluid flows, but converged in any other case).

The amine makeup stream (actually water) was inserted to help the convergence (while still simulating a real plant feature): neither column of this section, in fact, can let out the MDA outside the cycle, leading to a potential build-up problem in the calculation. This issue does not affect the column-reactor loop of the first plant part, because no species can escape it either via the reactor third stage or the column bottoms.

This section recovers 99.98% of the fed ethylene (considering the original stream plus the recycle), has a heat input of 2109 kW and releases 1636 kW.

Sweet gas dehydration

Final dehydration is further needed to accomplish a polymer-grade purity. This could in principle be carried out by further water condensation, as described in the previous sections, but this would imply the use of higher pressure, with consequent additional duties, or cryogenic condensation, with further costs. Therefore, we opted for a pressure-swing adsorption.

The simulation of the PSA of water was carried out at two levels:

- in the general scope, as a single unit operation that reproduces the input stream except one third of the ethylene and all the water, that are re-routed to the CO_2 adsorber;

- in a separate calculation, as two adsorption zeolite beds working in parallel in a basic 4-steps cycle (**Figure 8**).

The rigorous time-dependent calculus was performed considering a stream of 2400 kmol/h of ethylene with 2 mol% water content. The pressure levels were set to 5 and 1 atm [69]. The bed size and void fraction were tentatively chosen to have negligible pressure drops.

The adsorption of water onto zeolite-3A was parametrized following the data reported in [70], where a Langmuir isotherm model is used. Data for ethylene captured into a very similar zeolite were retrieved in [71] and retrofitted via a Langmuir model, because these latter authors employed a different equation but the simulation software used foresees one correlation for each used solid, not for each adsorbed specie. Other parameters were provided in [72].

After checking the actual cyclic ethylene dehydration (downstream) and the periodic bed cleaning (on the return line side), the data were put back into the wider steady-state plant scope. The power needed to compress the recycle up to the CO_2 stripper pressure is 2550 kW_{el}, and the heat discharged to keep its temperature at 20 °C amounts to 2700 kW_{th}.

Final ethylene separation

The scope of this section is essentially the purification of ethylene, rather than the recovery of the little butadiene carried alongside. This has an appreciable impact on the distillation column configuration, because in principle to treat a feed stream at ambient temperature into a cryogenic unit operation only the condenser is needed, while to obtain both C_2 and C_4 products with good purities a reboiler should be added.

To obtain a good-purity ethylene, the main issue is letting off the light gases still remaining, *i.e.* hydrogen, carbon monoxide and methane. The strategy adopted was a partial column condenser with both liquid and vapor distillates. A limited number of equilibrium trays is needed to effectively purge

butylene in the bottoms (given its already low concentration in the feed stream), so the block was optimized according to the overall distillate flow and the fraction of the let-off vapor distillate, until an acceptable trade-off was reached between ethylene recovery and light gases purging (we considered methane as the key component of this group, **Figure 17)**. After this analysis, the column was set to work with an overall distillate to feed ratio of 0.97 mol/mol, of which 8% purge gas: the recovery of ethylene was about 90% and the impurities less than 400 ppm.

The high pressure of the PSA section (5 atm) was maintained, the calculated boiling point (PSRK EoS) at the condenser was -71 °C, in very good agreement with the data published in [73], and its duty 6640 kW_{th}. The calculated K_{vl} for methane and ethylene were respectively, 11.8 and 1.0, fully compliant with experimental data [74].

Following a different approach with respect to the others plant sections, an energetic assessment of this sub-system was accomplished, because in this case the cooling utility is not at ambient temperature, according to the following steps:

- with the chosen mass balances, the bottoms are calculated to be at -60 °C, then they can be taken as an auxiliary heat sink with respect to the incoming feed;
- allowing a temperature difference as high as 20 °C for the gaseous feed cooling utility, it can be foreseen a cooldown to -40 °C releasing 1116 kW, then the column condenser has actually to release only 5534 kW;
- taking advantage of the distillate overpressure, its expansion to the atmospheric level yields a vapor fraction of 0.17 kg/kg (0.18 interpolating from [73]) and a saturation temperature of -104 °C (-105°C, ibid.) – allowing a temperature difference of 7 °C (condensing-boiling heat transfer) the ethylene stream can be turned into dry vapor at -78 °C absorbing 4924 kW;
- the remaining 611 kW can be transferred to a saturated ethylene stream (at atmospheric pressure) vaporizing 1.26 kg/s, which means to pass from $x = 0.11$ to $x = 0$ over the foreseen basis of 11.36 kg/s;

- to obtain this vapor title (h = -233 kJ/kg taking the reference state as in [75]) after an expansion, fixing the upstream temperature at 20 °C (lowest target for regular cooling utilities) it is obtained a pressure of 64 bar for the compressor (this point is actually beyond the experimental data so far cited, yet the calculation of the PSRK model is in very good agreement with the predictions reported in [76]).

The solution sketched above is reported synthetically on the ethylene phase chart in **Figure 20** (drew using the NIST REFPROP model – provided within the Aspen Plus suite – and reference state). The heated ethylene is still capable, together with the column bottoms and the purge gas, to cool down the feed stream in a feasible counter-counter exchange with a LMTD of 50 °C at the pinch point, which leaves wide optimization margins. The power input of 5860 kW_{el} and the heat release of 6720 kW_{th} let foresee a cryogenic efficiency of 48%.

Finally, the full details of all blocks and stream tables are reported in **Table 7**, **Table 9**, **Table 8, Table 10, Table 11, Table 12**. Overall, setting a target yield of 105 t/year of polymer-grade ethylene, the reactive section must be fed with 76 t/h of diluted ethanol and operated below 400 °C. The energy input amounts to 17 MW_{el} plus 73 MW_{th}.

Conclusions

Summarizing the results, the adopted kinetic model and its parametrization in light of the reviewed literature let foresee the following material distribution (**Figure 18**): 85% of the fed carbon mass is found as ethylene, 12% remains as ethanol and a 2% as higher olefins. Considering also the recycle of ethanol that comes from the condensation sections, the carbon conversion increases to the value of 97.6%.

The global ethylene recovery is 90.7%: most of the loss takes place in the last stage due to the non-condensable purification and to the adopted strategy of having low reflux ratio – and then a closed cryogenic balance – in the last purification column (**Figure 18**).

Dividing the simulation into independent sections offered some conceptual and practical advantages. Multipurpose gas-treating solutions, as the amine-sweetening and the pressure-swing adsorption, can be further refined and adapted to the needs of other plant types, avoiding that their more demanding calculations have a direct impact on each simulation convergence: the general simulations can integrate their results under simplified mass balances. Even without performing the energetic assessment of the whole plant, the demand for a cryogenic heat sink in the last section could be isolated and solved (**Figure 19**).

The adoption of a kinetic model for ethylene formation suggests how should the catalyst be managed. Much important, the activation energies of the reactions are instrumental to select the best inlet temperatures for the different reaction stages. While the reacting mixture loses heat almost linearly with respect to the ethanol conversion, the temperature within a single stage has a roughly exponential profile, so that loading the active material within solids of different densities, or at different void fractions, could help to smooth the thermal stresses.

The thermodynamic issues were answered with the help of literature data for every plant section: further refinements for very specific points (*e.g.* the water-MDA VLE or the Langmuir parameters in a zeolite bed) can still have an impact on a detailed block sizing, much less on the overall balances already assessed. In light of the results presented, the choice of the model has a sensible impact on the size and the energetic balances of the separation sections, less on the overall mass balances. When the reactor is not operated at 100% conversion, it is also important that the kinetic and thermodynamic models can predict the relative amount of condensable (ethanol, diethyl ether, acetaldehyde) and non-condensable (CO_2, hydrogen, olefins) byproducts.

In the framework of an integrated bio-refinery plant, the ethanol concentration can be shifted from the reactor inlet to the recycle. If the energy recovery is properly managed, the relatively high dew point of the ethylene-water mixture allows a product-feed heat exchange that makes up for the extra-heat apparently needed when diluted ethanol is fed. This latter options feature a larger condensation heat (at relatively low temperatures) at the first ethylene separator, but an upstream distillation column would still have a comparable condenser duty.

The presented simulation represents a step further with respect to others reviewed work: while the main results (ethanol conversion, ethylene purity, reaction and separation temperature ranges) are in line with the cited literature, the higher detail of this calculation in light of the data and models makes it flexible and reliable at the same time. On the other hand, when a reaction kinetic built upon laboratory tests is matched to plant surveys, discrepancies arise: this implies that also theoretical and experimental works on catalysts can benefit from a larger scale feedback to give more comprehensive models, adapted to wider ranges of reactor-management.

ABBREVIATIONS LIST

AP Aspen Plus

EoS Equation of State

NRTL Non-Random Two-Liquids model for activity coefficient

ENRTL Electrolyte Non-Random Two-Liquids model for activity coefficient

RK Redlich-Kwong equation of state

PSRK Predictive-Redlich-Kwong-Soave model

LHHW Langmuir-Hinshelwood-Hougen-Watson kinetic model

VLE Vapor Liquid Equilibrium

MDA N-Methyldiethanolamine

PSA Pressure Swing Adsorption

GHSV Gas Hourly Space Velocity

LMTD Log Mean Temperature Difference

Bibliography

(1) Koçar, G.; Civaş, N. *An Overview of Biofuels from Energy Crops: Current Status and Future Prospects*. *Renew. Sustain. Energy Rev.* **2013**, *28*, 900–916. https://doi.org/10.1016/j.rser.2013.08.022.

(2) Jong, E. De; Jungmeier, G. *Biorefinery Concepts in Comparison to Petrochemical Refineries*. In *Industrial Biorefineries and White Biotechnology*; Ashok Pandey, Höfer, R., Taherzadeh, M., Nampoothiri, M., Larroche, C., Eds.; Elsevier B.V, 2015; pp 3–33. https://doi.org/10.1016/B978-0-444-63453-5.00001-X.

(3) Posen, I. D.; Griffin, W. M.; Matthews, H. S.; Azevedo, I. L. *Changing the Renewable Fuel Standard to a Renewable Material Standard: Bioethylene Case Study*. *Environ. Sci. Technol.* **2015**, *49* (1), 93–102. https://doi.org/10.1021/es503521r.

(4) Horvath, I.; Csefalvay, E.; Mika, L.; Debreczeni, M. *Sustainability Metrics for Biomass-Based Carbon Chemicals*. *ACS Sustain. Chem. Eng.* **2017**, *5* (3), 2734–2740. https://doi.org/10.1021/acssuschemeng.6b03074.

(5) Machado, C. F. R.; Araújo, O. de Q. F.; de Medeiros, J. L.; Alves, R. M. de B. *Carbon Dioxide*

and Ethanol from Sugarcane Biorefinery as Renewable Feedstocks to Environment-Oriented Integrated Chemical Plants. J. Clean. Prod. **2018**, *172*, 1232–1242. https://doi.org/10.1016/j.jclepro.2017.10.234.

(6) Gallo, J. M. R.; Bueno, J. M. C.; Schuchardt, U. *Catalytic Transformations of Ethanol for Biorefineries. J. Braz. Chem. Soc.* **2014**, *25* (12), 2229–2243. https://doi.org/10.5935/0103-5053.20140272.

(7) Sun, J.; Wang, Y. *Recent Advances in Catalytic Conversion of Ethanol to Chemicals*. *ACS Catal.* **2014**, *4*, 1078–1090. https://doi.org/10.1080/01614940.2013.816610.

(8) Yang, M.; Tian, X.; You, F. *Manufacturing Ethylene from Wet Shale Gas and Biomass: Comparative Technoeconomic Analysis and Environmental Life Cycle Assessment*. *Ind. Eng. Chem. Res.* **2018**, *57* (17), 5980–5998. https://doi.org/10.1021/acs.iecr.7b03731.

(9) Arvidsson, M.; BJORN, L. Process Integration Study of a Biorefinery Producing Ethylene from Lignocellulosic Feedstock for a Chemical Cluster, Chalmers University of Technology, Goteborg (SE), 2011.

(10) Zhang, M.; Yu, Y. *Dehydration of Ethanol to Ethylene*. *Ind. Eng. Chem. Res.* **2013**, *52* (28), 9505–9514. https://doi.org/10.1021/ie401157c.

(11) Rossetti, I.; Compagnoni, M.; Finocchio, E.; Ramis, G.; Di Michele, A.; Millot, Y.; Dzwigaj, S. *Ethylene Production via Catalytic Dehydration of Diluted Bioethanol: A Step towards an Integrated Biorefinery*. *Appl. Catal. B Environ.* **2017**, *210*, 407–420.

(12) Morschbacker, A. *Bio-Ethanol Based Ethylene*. *Polym. Rev.* **2009**, *49* (2), 79–84. https://doi.org/10.1080/15583720902834791.

(13) Haro, P.; Ollero, P.; Trippe, F. *Technoeconomic Assessment of Potential Processes for Bio-Ethylene Production*. *Fuel Process. Technol.* **2013**, *114*, 35–48.

https://doi.org/10.1016/j.fuproc.2013.03.024.

(14) Gerssen-Gondelach, S. J.; Saygin, D.; Wicke, B.; Patel, M. K.; Faaij, A. P. C. *Competing Uses of Biomass: Assessment and Comparison of the Performance of Bio-Based Heat, Power, Fuels and Materials*. *Renew. Sustain. Energy Rev.* **2014**, *40* (April), 964–998. https://doi.org/10.1016/j.rser.2014.07.197.

(15) Zabed, H.; Sahu, J. N.; Suely, A.; Boyce, A. N.; Faruq, G. *Bioethanol Production from Renewable Sources: Current Perspectives and Technological Progress*. *Renew. Sustain. Energy Rev.* **2017**, *71* (January), 475–501. https://doi.org/10.1016/j.rser.2016.12.076.

(16) Liptow, C.; Tillman, A. M.; Janssen, M.; Wallberg, O.; Taylor, G. A. *Ethylene Based on Woody Biomass - What Are Environmental Key Issues of a Possible Future Swedish Production on Industrial Scale*. *Int. J. Life Cycle Assess.* **2013**, *18* (5), 1071–1081. https://doi.org/10.1007/s11367-013-0564-6.

(17) Muñoz, I.; Flury, K.; Jungbluth, N.; Rigarlsford, G.; I Canals, L. M.; King, H. *Life Cycle Assessment of Bio-Based Ethanol Produced from Different Agricultural Feedstocks*. *Int. J. Life Cycle Assess.* **2014**, *19* (1), 109–119. https://doi.org/10.1007/s11367-013-0613-1.

(18) Vohra, M.; Manwar, J.; Manmode, R.; Padgilwar, S.; Patil, S. *Bioethanol Production: Feedstock and Current Technologies*. *J. Environ. Chem. Eng.* **2014**, *2* (1), 573–584. https://doi.org/10.1016/j.jece.2013.10.013.

(19) Aditiya, H. B.; Mahlia, T. M. I.; Chong, W. T.; Nur, H.; Sebayang, A. H. *Second Generation Bioethanol Production: A Critical Review*. *Renew. Sustain. Energy Rev.* **2016**, *66*, 631–653. https://doi.org/10.1016/j.rser.2016.07.015.

(20) Lennartsson, P. R.; Erlandsson, P.; Taherzadeh, M. J. *Integration of the First and Second Generation Bioethanol Processes and the Importance of By-Products*. *Bioresour. Technol.* **2014**, *165* (C), 3–8. https://doi.org/10.1016/j.biortech.2014.01.127.

(21) Cook, D.; Hodge, S.; Moffatt, C. *Ethanol-to-Ethylene Process Provides Alternative Pathway to Plastics*. *Hydrocarb. Process.* **2014**, *July*, https://www.hydrocarbonprocessing.com/magazine/201.

(22) Jernberg, J.; Nørregård, Ø.; Olofsson, M.; Persson, O.; Thulin, M.; Hulteberg, C.; Karlsson, H. *Ethanol Dehydration to Green Ethylene*. **2015**, No. May.

(23) Ethylene from Ethanol, Chematur Engineering AB https://chematur.se/technologies/bio-chemicals/bio-ethylene-ethene/.

(24) Hu, Y. C. *Unconventional Olefin Processes*. *Hydrocarb. Process.* **1983**, *62* (5), 88–95.

(25) Kochar, N. K.; Merims, R.; Padia, A. S. *Ethylene from Ethanol*. *Chem. Eng. Process.* **1981**, *77* (6), 66–70.

(26) Ondrey, G. The Launch of a New Bioethylene-Production Process. *Chemical Engineering*. 2014, p https://www.chemengonline.com/the-launch-of-a-new-.

(27) Fan, D.; Dai, D. J.; Wu, H. S. *Ethylene Formation by Catalytic Dehydration of Ethanol with Industrial Considerations*. *Materials (Basel).* **2013**, *6* (1), 101–115. https://doi.org/10.3390/ma6010101.

(28) Voegele, E. Feeding the Chemical Market http://ethanolproducer.com/articles/8617/feeding-the-chemical-market.

(29) Mohsenzadeh, A.; Zamani, A.; Taherzadeh, M. J. *Bioethylene Production from Ethanol : A Review and Techno-Economical Evaluation*. *ChemBio Eng. Rev.* **2017**, No. 2, 75–91. https://doi.org/10.1002/cben.201600025.

(30) Knaeble, W.; Iglesia, E. *Kinetic and Theoretical Insights into the Mechanism of Alkanol Dehydration on Solid Brønsted Acid Catalysts*. *J. Phys. Chem. C* **2016**, *120*, 3371–3389. https://doi.org/10.1021/acs.jpcc.5b11127.

(31) Alexopoulos, K.; John, M.; Borght, K. Van Der; Galvita, V.; Reyniers, M.; Marin, G. B. *DFT-Based Microkinetic Modeling of Ethanol Dehydration in H-ZSM-5*. *J. Catal.* **2016**, *339*, 173–185. https://doi.org/10.1016/j.jcat.2016.04.020.

(32) DeWilde, J. F.; Chiang, H.; Hickman, D. A.; Ho, C. R.; Bhan, A. *Kinetics and Mechanism of Ethanol Dehydration on Al 2O3: The Critical Role of Dimer Inhibition*. *ACS Catal.* **2013**, *3* (4), 798–807. https://doi.org/10.1021/cs400051k.

(33) Christiansen, M. a.; Mpourmpakis, G.; Vlachos, D. G. *DFT-Driven Multi-Site Microkinetic Modeling of Ethanol Conversion to Ethylene and Diethyl Ether on γ-Al2O3(111)*. *J. Catal.* **2015**, *323*, 121–131. https://doi.org/10.1016/j.jcat.2014.12.024.

(34) Sutton, J. E.; Panagiotopoulou, P.; Verykios, X. E.; Vlachos, D. G. *Combined DFT, Microkinetic, and Experimental Study of Ethanol Steam Reforming on Pt*. *J. Phys. Chem. C* **2013**, *117* (9), 4691–4706. https://doi.org/10.1021/jp312593u.

(35) Wang, J. H.; Lee, C. S.; Lin, M. C. *Mechanism of Ethanol Reforming: Theoretical Foundations*. *J. Phys. Chem. C* **2009**, *113* (16), 6681–6688. https://doi.org/10.1021/jp810307h.

(36) DeWilde, J. F.; Czopinski, C. J.; Bhan, A. *Ethanol Dehydration and Dehydrogenation on Al2O3: Mechanism of Acetaldehyde Formation*. *ACS Catal.* **2014**, *4* (12), 4425–4433. https://doi.org/10.1021/cs501239x.

(37) Rossetti, I.; Compagnoni, M.; De Guido, G.; Pellegrini, L. A.; Ramis, G.; Dzwigaj, S. *Ethylene Production from Diluted Bioethanol Solutions*. *Can. J. Chem. Eng.* **2017**, *95* (9), 1752–1759. https://doi.org/10.1002/cjce.22828.

(38) Chang, C. L.; Devera, A. L.; Miller, D. J. *A Lumped Kinetic Model for Dehydration of Ethanol to Hydrocarbons over Hzsm-5*. *Chem. Eng. Commun.* **1990**, *95* (1), 27–39. https://doi.org/10.1080/00986449008911464.

(39) Derouane, E. G.; Nagy, J. B.; Dejaifve, P.; van Hooff, J. H. C.; Spekman, B. P.; Védrine, J. C.; Naccache, C. *Elucidation of the Mechanism of Conversion of Methanol and Ethanol to Hydrocarbons on a New Type of Synthetic Zeolite*. *J. Catal.* **1978**, *53* (1), 40–55. https://doi.org/10.1016/0021-9517(78)90006-4.

(40) Lee, J.; Szany, J.; Kwak, J. H. *Ethanol Dehydration on G-Al2O3: Effects of Partial Pressure and Temperature*. *Mol. Catal.* **2017**, *434*, 39–48.

(41) Tripodi, A.; Compagnoni, M.; Martinazzo, R.; Ramis, G.; Rossetti, I. *Process Simulation for the Design and Scale Up of Heterogeneous Catalytic Process: Kinetic Modelling Issues*. *Catalysts* **2017**, *7*. https://doi.org/10.3390/catal7050159.

(42) Kang, M.; Bhan, A. *Kinetics and Mechanisms of Alcohol Dehydration Pathways on Alumina*. *Catal. Sci. Technol.* **2016**, *6*, 6667–6678. https://doi.org/10.1039/C6CY00990E.

(43) Becerra, J.; Figueredo, M.; Cobo, M. *Thermodynamic and Economic Assessment of the Production of Light Olefins from Bioethanol*. *J. Environ. Chem. Eng.* **2017**, *5* (2), 1554–1564. https://doi.org/10.1016/j.jece.2017.02.035.

(44) Le, L.; Nagulapalli, N.; Cameron, G.; Levine, J. *Process Design for the Production of Ethylene from Ethanol*. *Sr. Des. Reports* **2012**, *39*, 1–144.

(45) Nitzsche, R.; Budzinski, M.; Gröngröft, A. *Techno-Economic Assessment of a Wood-Based Biorefinery Concept for the Production of Polymer-Grade Ethylene, Organosolv Lignin and Fuel*. *Bioresour. Technol.* **2016**, *200*, 928–939. https://doi.org/10.1016/j.biortech.2015.11.008.

(46) Maia, J. G. S. S.; Demuner, R. B.; Secchi, A. R.; Melo, P. A.; Carmo, R. W. Do; Gusmão, G. S. *Process Modeling and Simulation of an Industrial-Scale Plant for Green Ethylene Production*. *Ind. Eng. Chem. Res.* **2018**, *57* (18), 6401–6416. https://doi.org/10.1021/acs.iecr.8b00776.

(47) Becerra, J.; Quiroga, E.; Tello, E.; Figueredo, M.; Cobo, M. *Kinetic Modeling of Polymer-Grade Ethylene Production by Diluted Ethanol Dehydration over H-ZSM-5 for Industrial Design*. *J. Environ. Chem. Eng.* **2018**, *6* (5), 6165–6174. https://doi.org/10.1016/j.jece.2018.09.035.

(48) Yakovleva, I. S.; Banzaraktsaeva, S. P.; Ovchinnikova, E. V.; Chumachenko, V. A.; Isupova, L. A. *Catalytic Dehydration of Bioethanol to Ethylene. Review. Katal. v promyshlennosti* **2016**, *16* (1), 57–73. https://doi.org/10.18412/1816-0387-2016-1-57-73.

(49) Kagyrmanova, A. P.; Chumachenko, V. A.; Korotkikh, V. N.; Kashkin, V. N.; Noskov, A. S. *Catalytic Dehydration of Bioethanol to Ethylene: Pilot-Scale Studies and Process Simulation*. *Chem. Eng. J.* **2011**, *176–177*, 188–194. https://doi.org/10.1016/j.cej.2011.06.049.

(50) Maia, J. G. S. S.; Demuner, R. B.; Secchi, A. R.; Biscaia, E. C. *Modeling and Simulation of the Process of Dehydration of Bioethanol to Ethylene*. *Brazilian J. Chem. Eng.* **2016**, *33* (3), 479–490. https://doi.org/10.1590/0104-6632.20160333s20150139.

(51) Skinner, M. J.; Michor, E. L.; Fan, W.; Tsapatsis, M.; Bhan, A.; Schmidt, L. D. *Ethanol Dehydration to Ethylene in a Stratified Autothermal Millisecond Reactor*. *ChemSusChem* **2011**, *4* (8), 1151–1156. https://doi.org/10.1002/cssc.201100026.

(52) Tripodi, A.; Compagnoni, M.; Rossetti, I. *Kinetic Modeling and Reactor Simulation for Ethanol Steam Reforming*. *ChemCatChem* **2016**, *8*, 3804 – 3813. https://doi.org/10.1002/cctc.201601075.

(53) Barrocas, V.; da Silva, J.; de Assis, R. Process for Preparing Ethene. 4232179, 1980. https://doi.org/10.1057/9780230607156.

(54) Llano-Restrepo, M.; Muñoz-Muñoz, Y. M. *Combined Chemical and Phase Equilibrium for the Hydration of Ethylene to Ethanol Calculated by Means of the Peng-Robinson-Stryjek-Vera Equation of State and the Wong-Sandler Mixing Rules*. *Fluid Phase Equilib.* **2011**, *307* (1),

45–57. https://doi.org/10.1016/j.fluid.2011.05.007.

(55) Bae, H. K.; Nagahama, K. *Measurement and Correlation of High Vapor-Liquid Equilibria for the Systems Ethylene-1-Butene and Ethylene-Propylene*. **1981**, *14*, 1–6.

(56) *Solublity Data Serie - Volume 57*; Walter, H., Ed.; Oxford University Press: Oxford, 1994; Vol. 57, 1–375.

(57) IUPAC. *Solubility Data Series Volume 56-Alcohols with Hydrocarbons*. **1994**, *56*, *1–320*.

(58) Rufford, T. E.; Smart, S.; Watson, G. C. Y.; Graham, B. F.; Boxall, J.; Diniz da Costa, J. C.; May, E. F. *The Removal of CO2 and N2 from Natural Gas: A Review of Conventional and Emerging Process Technologies*. *J. Pet. Sci. Eng.* **2012**, *94–95*, 123–154. https://doi.org/10.1016/j.petrol.2012.06.016.

(59) Kohl, A.; Nielsen, R. B. *Gas Purification*, 5th ed.; Gulf Publishing Company: Houston, 1997.

(60) Yu, W. C.; Astarita, G.; Savage, D. W. *Kinetics of Carbon Dioxide Absorption in Solutions of Methyldiethanolamine*. *Chem. Eng. Sci.* **1985**, *40* (8), 1585–1590. https://doi.org/10.1016/0009-2509(85)80101-9.

(61) Simo, M.; Brown, C. J.; Hlavacek, V. *Simulation of Pressure Swing Adsorption in Fuel Ethanol Production Process*. *Comput. Chem. Eng.* **2008**, *32* (7), 1635–1649. https://doi.org/10.1016/j.compchemeng.2007.07.011.

(62) Aden, a; Ruth, M.; Ibsen, K.; Jechura, J.; Neeves, K.; Sheehan, J.; Wallace, B.; Montague, L.; Slayton, A.; Lukas, J. *Lignocellulosic Biomass to Ethanol Process Design and Economics Utilizing Co-Current Dilute Acid Prehydrolysis and Enzymatic Hydrolysis for Corn Stover*. *Natl. Renew. Energy Lab.* **2002**, No. June, Medium: ED; Size: 154 pages. https://doi.org/NREL/TP-510-32438.

(63) Phung, T. K.; Radikapratama, R.; Garbarino, G.; Lagazzo, A.; Riani, P.; Busca, G. *Tuning of*

Product Selectivity in the Conversion of Ethanol to Hydrocarbons over H-ZSM-5 Based Zeolite Catalysts. *Fuel Process. Technol.* **2015**, *3*. https://doi.org/10.1016/j.fuproc.2015.03.012.

(64) Banzaraktsaeva, S. P.; Ovchinnikova, E. V.; Isupova, L. A.; Chumachenko, V. A. *Catalytic Dehydration of Ethanol into Ethylene in a Tubular Reactor of the Pilot Installation on Alumina Catalysts with Varied Grain Size*. *Russ. J. Appl. Chem.* **2017**, *90* (2), 169–178. https://doi.org/10.1134/S1070427217020021.

(65) Ramis, G.; Rossetti, I.; Tripodi, A.; Compagnoni, M. *Diluted Bioethanol Solutions for the Production of Hydrogen and Ethylene*; 2017; Vol. 57. https://doi.org/10.3303/CET1757278.

(66) Skiba, E. A.; Baibakova, O. V; Budaeva, V. V; Pavlov, I. N.; Vasilishin, M. S.; Makarova, E. I.; Sakovich, G. V; Ovchinnikova, E. V; Banzaraktsaeva, S. P.; Vernikovskaya, N. V; et al. *Pilot Technology of Ethanol Production from Oat Hulls for Subsequent Conversion to Ethylene*. *Chem. Eng. J.* **2017**, *329*, 178–186. https://doi.org/10.1016/j.cej.2017.05.182.

(67) Gales, L.; Mendes, A.; Costa, C. *Recovery of Acetone, Ethyl Acetate and Ethanol by Thermal Pressure Swing Adsorption*. *Chem. Eng. Sci.* **2003**, *58* (23–24), 5279–5289. https://doi.org/10.1016/j.ces.2003.09.006.

(68) De Guido, G.; Compagnoni, M.; Pellegrini, L. A.; Rossetti, I. *Mature versus Emerging Technologies for CO2 Capture in Power Plants: Key Open Issues in Post-Combustion Amine Scrubbing and in Chemical Looping Combustion*. *Front. Chem. Sci. Eng.* **2018**, *12* (2), 315–325. https://doi.org/10.1007/s11705-017-1698-z.

(69) Luna, J. S.; Gomar-Madriz, L. E.; Castro-Montoya, A. J.; Serna-González, M.; Hernández-Castro, S. *Dehydration of Ethanol by PSA Process with Pressure Equalization Step Added*. *Bioethanol* **2016**, *2* (1), 76–83. https://doi.org/10.1515/bioeth-2016-0004.

(70) Kim, K. M.; Oh, H. T.; Lim, S. J.; Ho, K.; Park, Y.; Lee, C. H. *Adsorption Equilibria of Water Vapor on Zeolite 3A, Zeolite 13X, and Dealuminated y Zeolite*. *J. Chem. Eng. Data* **2016**, *61*

(4), 1547–1554. https://doi.org/10.1021/acs.jced.5b00927.

(71) Aguado, S.; Daniel, C.; Farrusseng, D.; Recherches, I. De; Ircelyon, D. L.; Einstein, A. A. *Absolute Molecular Sieve Separation of Ethylene / Ethane Mixtures*. *J. Am. Chem. Soc.* **2012**, *134*, 14635–14637. https://doi.org/10.1021/ja305663k.

(72) Simo, M.; Sivashanmugam, S.; Brown, C. J.; Hlavacek, V. *Adsorption/Desorption of Water and Ethanol on 3A Zeolite in near-Adiabatic Fixed Bed*. *Ind. Eng. Chem. Res.* **2009**, *48* (20), 9247–9260. https://doi.org/10.1021/ie900446v.

(73) Buhner, K.; Maurer, G.; Bender, E. *Pressure-Enthalpy Diagrams for Methane, Ethane, Propane, Ethylene and Propylene*. *Cryogenics (Guildf).* **1981**, *100* (March), 157–164.

(74) Guter, M.; Newitt, D. M.; Ruhemann, M. *Two-Phase Equilibrium In Binary And Ternary Systems II. The System Methane-Ethylene III. The System Methane-Ethane-Ethylene*. *Proc. R. Soc. London A Math. Phys. Eng. Sci.* **1940**, *176* (964), 140–152. https://doi.org/10.1098/rspa.1940.0083.

(75) *ASHRAE Handbook - Fundamentals: Chapter 30, Thermophysical Properties of Refrigerants*; ASHRAE: Atlanta, 2017.

(76) Smukala, J.; Span, R.; Wagner, W. *New Equation of State for Ethylene Covering the Fluid Region for Temperatures From the Melting Line to 450 K at Pressures up to 300 MPa*. *J. Phys. Chem. Ref. Data* **2000**, *29* (5), 1053–1121.

(77) "Plant Status: Taiwan's Formosa Plastics," ICIS News, 2019. [Online]. Available: https://www.icis.com/explore/resources/news/2019/02/12/10317435/plant-status-taiwan-s-formosa-plastics-to-shut-eva-plant-on-18-feb/. [Accessed: 23-Apr-2019].

(78) "Nova Plant facilities," Nova Chemicals. [Online]. Available: http://www.novachem.com/Pages/joffre/joffre-plants.aspx. [Accessed: 23-Apr-2019].

(79) “Exxon Mobile Starts Up New ethane cracker in Baytown, TX,” 2018. [Online]. Available: https://news.exxonmobil.com/press-release/exxonmobil-starts-new-ethane-cracker-baytown-texas. [Accessed: 23-Apr-2019].

(80) Erpelding, J. J. Erpelding, “DowDuPont announces start-up of world-scale ethylene production facility,” The Dow Chemical Company, 2017. [Online]. Available: https://corporate.dow.com/en-us/news/press-releases/dow-announces-startup-of-worldscale-ethylene-production-faci.

(81) Tullo, A. “Notes On Dow’s Brazilian Biopolymers Project,” 2011. [Online]. Available: http://cenblog.org/the-chemical-notebook/2011/07/447/. [Accessed: 23-Apr-2019].

(82) “I’m Green Polyethylene.” [Online]. Available: http://plasticoverde.braskem.com.br/site.aspx/Im-greenTM-Polyethylene. [Accessed: 23-Apr-2019].

(83) Broeren, M. “Production of Bio-Ethylene,” IEA-ETSAP and IRENA, No. January, Pp. 1–9, 2013. *IEA-ETSAP and IRENA*. 2013, pp 1–9.

(84) Tardy, M. *“SOLVAY INDUPA WILL PRODUCE BIOETHANOL-BASED VINYL IN BRASIL,” Solvay Press Release, Https://Www.Chemeurope.Com/En/News/75840/Solvay-Indupa-Will-Produce-Bioethanol-Based-Vinyl-in-Brasil-Considers-State-of-the-Art-Power-Generation-in-Argentina.Html*; 2007.

(85) Pérez-Salado Kamps, Á.; Maurer, G. *Dissociation Constant of N -Methyldiethanolamine in Aqueous Solution at Temperatures from 278 K to 368 K . J. Chem. Eng. Data* **2002**, *41* (6), 1505–1513. https://doi.org/10.1021/je960141+.

Tables

Brute formula	Name	Cas n°
CH_4	methane	74-82-8
CO	Carbon monoxide	630-08-0
CO_2	Carbon dioxide	124-38-9
C_2H_6	ethane	74-84-0
C_2H_6O	Ethanol	64-17-5
C_2H_4	Ethylene	74-85-1
C_2H_5O	Acetaldehyde	75-07-0
$C_4H_{10}O$	Diethyl-ether	60-29-7
C_4H_8	1-butene	106-98-9
$C_5H_{13}O_2N$	Methyl-Diethanol-Amine (MDA)	105-59-9
H_2	Hydrogen	1333-74-0
H_2O	Water	7732-18-5

Table 1: List of the substances used for the plant simulation.

Model used	Database of model parameters	Sections
PSRK	APV90 EOS-LIT	Reaction, Olefins separation
NRTL-RK	APV90 VLE-RK	Separation
NRTL-RK – HENRY	APV90 VLE-RK – HENRY-AP/BINARY	Separation
ENRTL-RK	APV90 ENRTL-RK	CO2 absorption via amines

Table 2: List of the thermodynamic models and relative parameters databases used.

Reaction n°	Activation Energy [kJ/mol]	k^0 / $k^0_{(1)}$ $\frac{[\text{mol}\ g^{-1}\ s^{-1}]}{[\text{mol}\ g^{-1}\ s^{-1}]}$	Type
1	133	1.13×10^6	Forward
2	80	2.25×10^3	Forward

3	143	2.20×10^{6}	Forward
4	107	2.39×10^{3}	Forward
5	132	3.42×10^{5}	Forward
9	123	2.82×10^{-3}	Reversible
10	196	1.53×10^{-3}	Reversible

Table 3: Specifications for the reaction rates, with kinetic constants given as ratios to the first. Reactions are listed as in paragraph 0.

Data	Company	Location	**Yield (ton/year)**	**Reference**
Plant:	Formosa Plastics	Taiwan	2.7×10^{6}	[77]
Steam cracking	Nova Chemicals	Canada	2.9×10^{6}	[78]
	APC	Saudi Arabia	2.2×10^{6}	[27]
	Exxon Mobile	USA	1.3×10^{6}	[79]
	Dow DuPont	USA	$1.5 – 2.0 \times 10^{6}$	[80]
Plant:	Dow DuPont	Brazil	3.5×10^{5}	[81]
Bioethanol dehydration	Braskem	Brazil	2.0×10^{5}	[82]
	India Glycols Ltd	India	$<1.7 \times 10^{5}$	[83]
	Solvay	Brazil	6.0×10^{4}	[84]
Simulation:			1.0×10^{6}	[44]
Bioethanol dehydration			2.0×10^{5}	[9]
			1.8×10^{5}	[29]

Table 4: Some of the reviewed ethylene production capabilities. The Dow and Solvay Brazilian plant were not yet commissioned at the time the reference was accessed.

Specifications for the flash block V104			
T = 40 °C	P = 1.0 atm		
Specifications for the column V105			
Trays	10	Type	equilibrium
Feed tray	1 (top)	Condenser	None

Distillate	600 kmol/h	P (tray 1) = 1.0 atm	ΔP = 0.0 atm

Table 5: Simulation inputs for the separation blocks of the reactor recycle.

Reaction	Stoichiometry	$-\Delta H/_R$ (K)	$\Delta S/_R$	C	Reference
11	$2H_2O + CO_2 \rightleftarrows HCO_3^- + H_3O^+$	-12092	+231.46	-36.782	Aspen Plus database
12	$H_2O + MDAH^+ \rightleftarrows MDA + H_3O^+$	-820.00	-83.500	+10.970	Ref [85]
13	$2H_2O \rightleftarrows OH^- + H_3O^+$	-13446	+132.90	-22.477	Aspen Plus database

Table 6: Reactions for the amine-CO_2 section: the equilibrium constants are given according to the formulation: $K = (T^C)e^{-\Delta G/_{RT}}$

	Mass flows (t/h)					Energy flows (MW)	
	Ethanol	**Water**	**Ethylene**	**Lights**	**Heavies**	**Heat**	**Work**
Section 1 input	77.8	91.5	0.7	0.00	0.33	+70.4	-
Section 1 output	1.86	121	46.0	0.023	1.57	-36.5	-
Section 2 input	1.80	2.38	46.0	0.023	1.57	-	+7.57
Section 2 output	1.80	2.38	46.0	0.023	1.57	-4.70	-
Section 3 input	0.00	0.556	67.4	0.026	2.09	+2.11	+2.55
Section 3 output	0.00	0.556	67.4	0.026	2.09	-4.33	-
Section 4 input	0.00	0.164	67.0	0.022	2.09	-	-
Section 4 output	0.00	0.164	67.0	0.022	2.09	-	-
Section 5 input	0.00	0.00	44.9	0.019	0.39	-	+5.86
Section 5 output	0.00	0.00	44.9	0.019	0.39	-6.72	-
Plant input	**+76.0**	**+89.2**	**+0.00**	**+0.00**	**+0.00**	**+72.5**	**+16.0**
Plant output	**-0.00**	**-31.7**	**-44.9**	**-0.023**	**-1.24**	**-47.5**	**-0.00**

Table 7: Mass and energy balances. The recompression and cooling duties of section 4 recycle are added to section 3 balance.

Name	Description	Power	Heat input	Heat output	Moles generated	ΔP	Split fraction 1:2
		MW	MW	MW	kmol/h	bar	kg/kg
V101	First reactor stage	-	-	-	+620	-	1.00
V102	Second reactor stage	-	-	-	+592	-	1.00
V103	Third reactor stage	-	-	-	+411	-	1.00
V104	Flash separator	-	-	-	-	-	0.38
V105	Ethanol recovery column	-	15.76	-	-	-	0.11
H106	Feed-product heat exchanger	-	70.27	70.27	-	-	-
H107	Feed heater	-	48.25	-	-	-	-
H108	Reheater	-	14.51	-	-	-	-
H109	Reheater	-	7.63	-	-	-	-
H110	Column reboiler	-	-	15.76	-	-	0.21
H111	Product condenser	-	-	36.48	-	-	-
Section 1	**neat Energy Balance**	**0.0**	**70.39**	**36.48**	**-**	**-**	**-**
C201	1st product compressor	1.35	-	-	-	+1.0	-
C202	2nd product compressor	1.15	-	-	-	+2.0	-
C203	3rd product compressor	1.12	-	-	-	+4.0	-
C204	4th product compressor	1.08	-	-	-	+8.0	-
V205	1st water separator	-	-	-	-	-	14
V206	2nd water separator	-	-	-	-	-	90
V207	3rd water separator	-	-	-	-	-	101
V208	4th water separator	-	-	-	-	-	113
H209	1st water condenser	-	-	3.52	-	-	-
H210	2nd water condenser	-	-	1.38	-	-	-
H211	3rd water condenser	-	-	1.33	-	-	-
H212	4th water condenser	-	-	1.34	-	-	-
Section 2	**neat Energy Balance**	**4.7**	**0.0**	**7.57**	**-**	**-**	**-**

V301	CO_2 stripper	-	-	-	-	-	8.33
V302	Amine regenerator	-	-	-	-	-	0.43
V303	Regenerator water separator	-	-	-	-	-	0.40
H304	Rich-amine preheater	-	0.48	0.48	-	-	-
H305	Regenerator steam boiler	-	2.11	-	-	-	0.51
H306	Regenerator steam condenser	-	-	1.64	-	-	-
A307	Pressure regulator	-	-	-	-	-14.0	-
P308	Lean amine pump	<0.01	-	-	-	+14.0	-
Section 3	**neat Energy Balance**	**0.0**	**2.11**	**1.64**	**-**	**-**	**-**
V501	Ethylene column	-	-	-	-	-	57.9
V502	Lights separator	-	-	-	-	-	0.08
C503	Ethylene compressor	5.86	-	-	-	+64.0	-
H504	Feed cooler	-	1.04	1.04	-	-	-
H505	Feed cooler	-	0.074	0.074	-	-	-
H506	Ethylene condenser	-	0.61	0.61	-	-	-
H507	Ethylene condenser	-	4.92	4.92	-	-	-
H508	Ethylene cooler	-	-	6.72	-	-	-
A509	1^{st} throttling valve	-	-	-	-	-4.0	-
A510	2^{nd} throttling valve	-	-	-	-	-64.0	-
Section 5	**neat Energy Balance**	**5.86**	**0.0**	**6.72**	**-**	**-**	**-**

Table 8: Main working data of the process blocks. The split fractions are given as the proportion between the lighter and the heavier stream.

Stream	101	102	110	111	120	121	122	123	124	125	126	127	128	129	130	131	132	134	135
P (atm)	1.0	4.0	1.0	1.0	1.0	1.0	1.0	1.0	1.0	1.0	1.0	1.0	1.0	1.0	1.0	1.0	1.0	1.0	1.0
T (°C)	20.0	49.0	40.0	100.0	91.0	430.0	352.0	304.0	430.0	365.0	430.0	286.0	245.0	85.0	40.0	40.0	90.0	99.8	100.0
Mass Flow (t/h)	165.0	5.03	51.4	118.7	165.0	165.0	165.0	187.5	187.5	187.5	187.5	187.5	187.5	187.5	187.5	135.0	16.4	143.8	25.1
Ethanol	76.0	1.67	1.80	0.057	76.0	76.0	47.1	58.0	58.0	30.4	30.4	11.1	11.1	11.1	11.1	9.27	9.22	.215	.157
Water	89.2	2.35	2.38	119.0	89.2	89.2	100.0	110.0	110.0	121.0	121.0	128.0	128.0	128.0	128.0	126.0	7.19	143.6	24.9
Ethylene	0	.724	46.0	0	0	0	17.4	18.4	18.4	35.0	35.0	46.2	46.2	46.2	46.2	.002	.016	0	0
Lights	0	0	.023	0	0	0	.010	.010	.010	.019	.019	.023	.023	.023	.023	0	0	0	0
Heavies	0	.290	1.57	0	0	0	.278	.545	.545	.834	.834	1.08	1.08	1.08	1.08	.029	.010	0	0

Table 9: Stream report for the first section (see also **Figure 6**). Slight discrepancies might arise from rounding-up.

Stream	201	210	211	220	221	222	223	224	225	226	227	228	229	230	231	232	233	234
P (atm)	1.0	16.0	2.0	2.0	2.0	2.0	4.0	4.0	4.0	8.0	8.0	8.0	16.0	16.0	16.0	8.0	4.0	2.0
T (°C)	40.0	20.0	20.0	96.3	20.0	20.0	74.8	20.0	20.0	75.0	20.0	20.0	75.5	20.0	20.0	20.0	20.0	20.0
Mass Flow (t/h)	51.4	46.4	5.03	51.4	51.4	47.8	47.8	47.8	47.3	47.3	47.3	46.8	46.8	46.8	.411	.465	.530	3.52
Ethanol	1.80	.129	1.67	1.80	1.80	.776	.776	.776	.527	.527	.527	.290	.290	.290	.161	.237	.248	1.02
Water	2.38	.010	2.35	2.38	2.38	.291	.291	.291	.117	.117	.117	.042	.042	.042	.030	.077	.174	2.07
Ethylene	46.0	45.2	.724	46.0	46.0	45.5	45.5	45.5	45.4	45.4	45.4	45.3	45.3	45.3	.168	.118	.087	.351
Lights	.023	.023	0	.023	.023	.023	.023	.023	.023	.023	.023	.023	.023	.023	0	0	0	0
Heavies	1.57	1.11	.290	1.57	1.57	1.21	1.21	1.21	1.19	1.19	1.19	1.16	1.16	1.16	.054	.033	.021	.074

Table 10: Stream report for the second section (see also **Figure 6**). Slight discrepancies might arise from rounding-up.

Stream	**301**	**302**	**303**	**310**	**311**	**320**	**321**	**322**	**323**	**324**	**325**	**326**	**327**	**328**	**329**	**330**	**331**
P (atm)	15	15	15	15	1.0	15	15	1.0	1.0	15	15	15					
T (°C)	20.0	20.0	20.0	32.0	87.9	29.0	82.6	82.6	99.6	100	39.0	38.4	99.6	99.6	96.2	87.9	87.9
pH	-	-	-	-	-	9.3	8.3	8.3	8.8	8.8	9.9	9.9	-	-	-	-	-
Mass Flow (t/h)	46.4	22.1	0.54	67.8	1.28	8.13	8.13	8.13	6.85	6.85	6.85	7.39	10.4	3.51	4.46	4.46	3.18
Water	.010	.006	0.54	.164	.376	6.88	6.88	6.88	6.50	6.50	6.50	7.04	9.76	3.26	2.72	2.72	2.34
Ethylene	45.2	22.1	0	67.3	.013	.013	.013	.013	0	0	0	0	0	0	.013	.013	0
CO_2-HCO_3^-	.0044	0	0	ppm	.0044	.0075	.0075	.0075	.0014	.0014	.0014	.0015	.0019	.0005	0.0044	0.0044	0
MDA-$MDAH^+$	0	0	na	ppm	ppb	.113	.113	.113	.113	.113	.113	.113	.113	ppm	ppm	ppm	ppm
Lights	.022	0	0	.022	<ppm	<ppm	<ppm	<ppm	<ppm	<ppm	<ppm	<ppm	0	0	<ppm	<ppm	0
Heavies	1.24	0	0	.340	.900	.941	.941	.941	.041	.041	.041	.041	.491	.450	1.76	1.76	.864

Table 11: Stream report for the third section (see also **Figure 7**). Slight discrepancies might arise from rounding-up; for the CO_2 - HCO_3^- couple, the mass balance is affected appreciably by the OH addition.

Stream	501	510	511	512	520	521	522	523	524	525	526	527	528	529	530	531	532	533	534
P (atm)	5.0	1.0	5.0	5.0	5.0	5.0	5.0	5.0	5.0	5.0	5.0	1.0	1.0	65	65	1.0	1.0	1.0	5.0
T (°C)	20	-25	-25	-71	-36	-40	-70	-70	-71	-71	-71	-104	-78	240	22	-104	-95	-61	-71
Mass Flow (t/h)	45.3	40.9	.858	3.53	45.3	45.3	49.7	49.7	49.7	46.2	40.9	40.9	40.9	40.9	40.9	40.9	40.9	.858	5.26
Ethylene	44.9	40.9	.472	3.52	44.9	44.9	49.7	49.7	49.7	46.1	40.9	40.9	40.9	40.9	40.9	40.9	40.9	.472	5.26
Lights	.019	.009	ppm	.010	.019	.019	.018	.018	.018	.017	.015	.015	.015	.015	.015	.015	.015	ppm	.002
Heavies	.393	.007	.386	ppm	.393	.393	.008	.008	.008	.008	.007	.007	.007	.007	.007	.007	.007	.386	.001

Table 12: Stream report for the last section (see also **Figure 9Figure 7**). Slight discrepancies might arise from rounding-up. Notice that the results of section 4 are considered directly as a difference between streams ‘310’ and ‘501’.

Figures

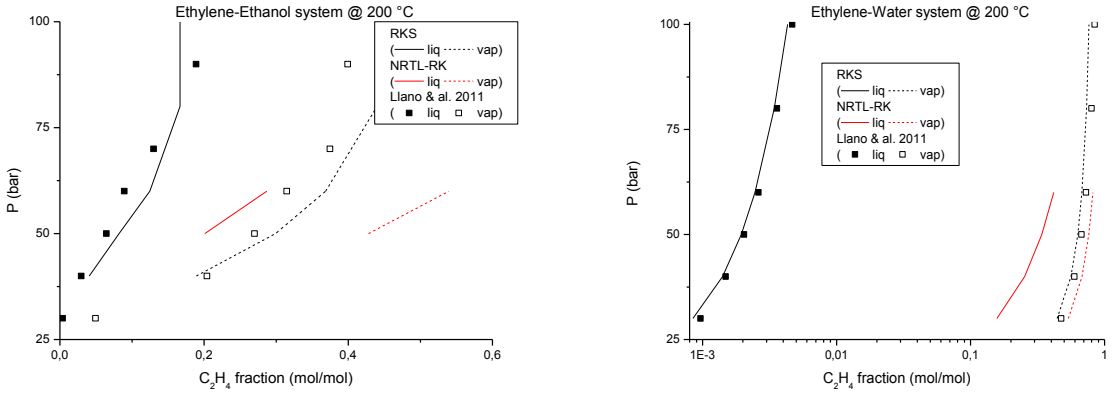

Figure 1: Ethylene-ethanol and ethyelene-water VLE.

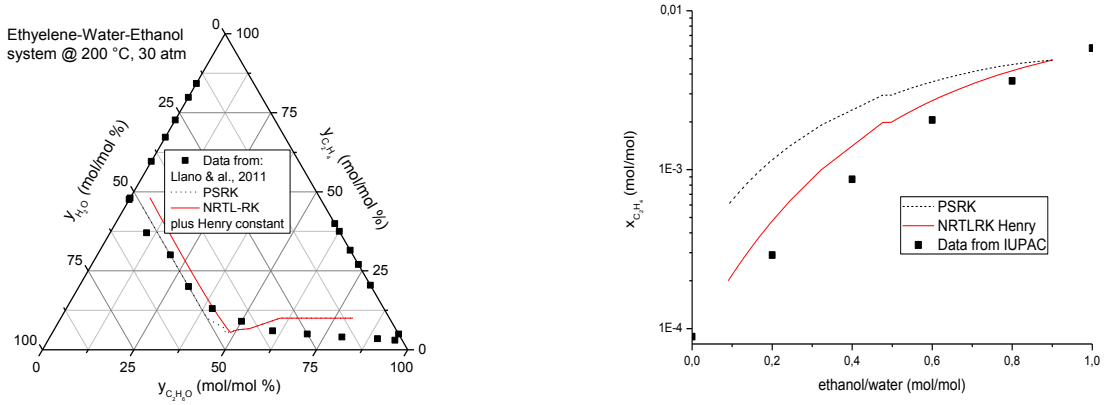

Figure 2: VLE between ethanol-ethylene and water at 30 bar (left) and ambient conditions (right).

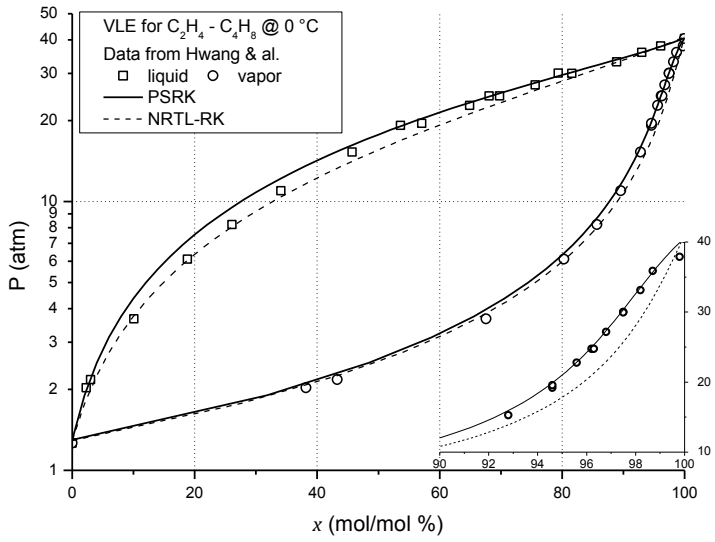

Figure 3: VLE for ethylene and butene at 0 °C; inset: the liquid at high ethylene content.

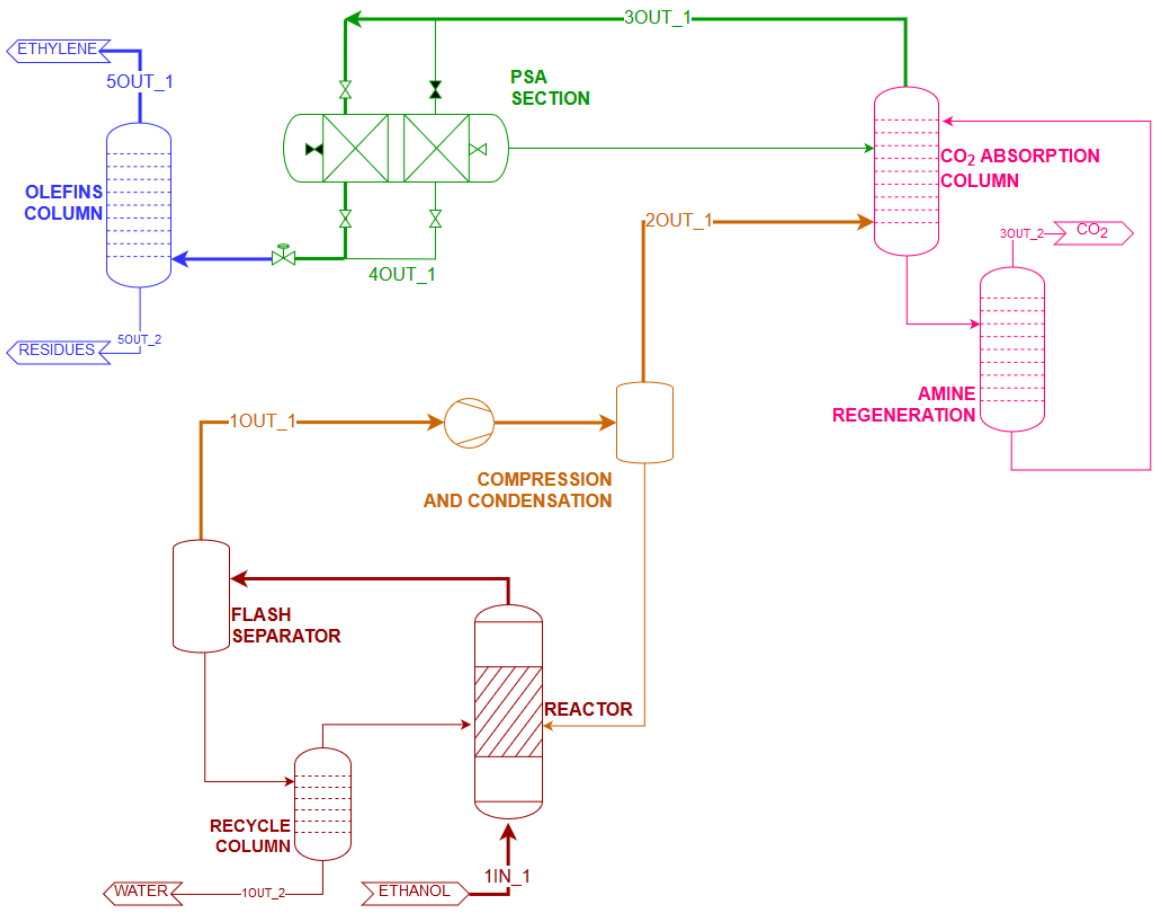

Figure 4: General layout for an ethanol-ethylene plant.

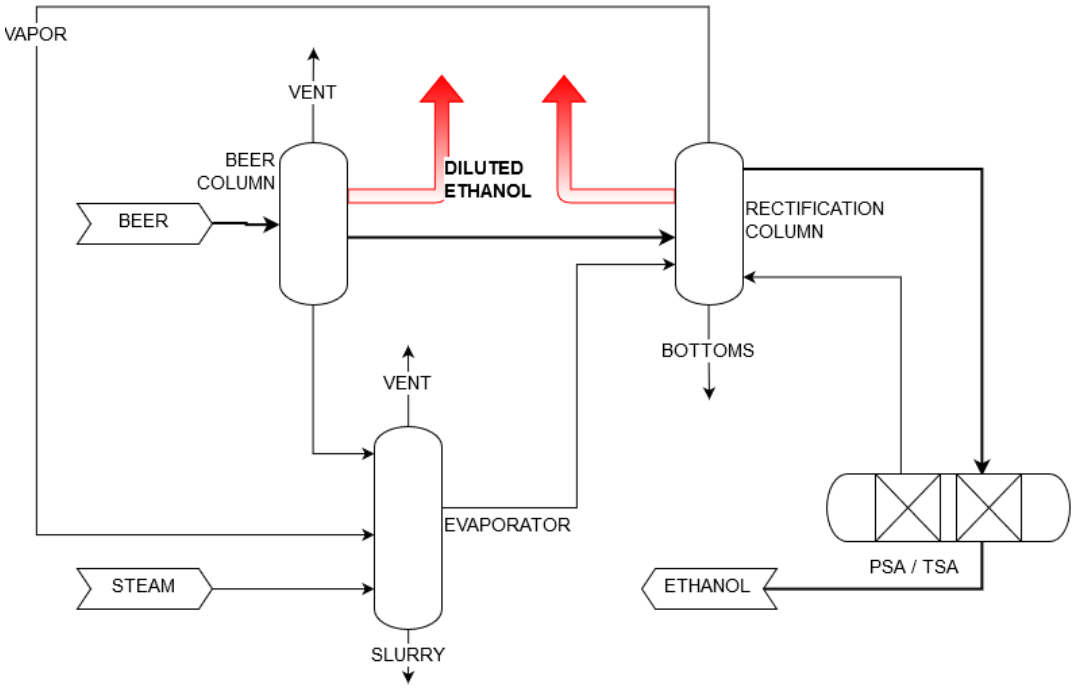

Figure 5: Possible touring of diluted bioethanol to an ethylene reactor. The scheme is derived by a comparison of [9,45,62].

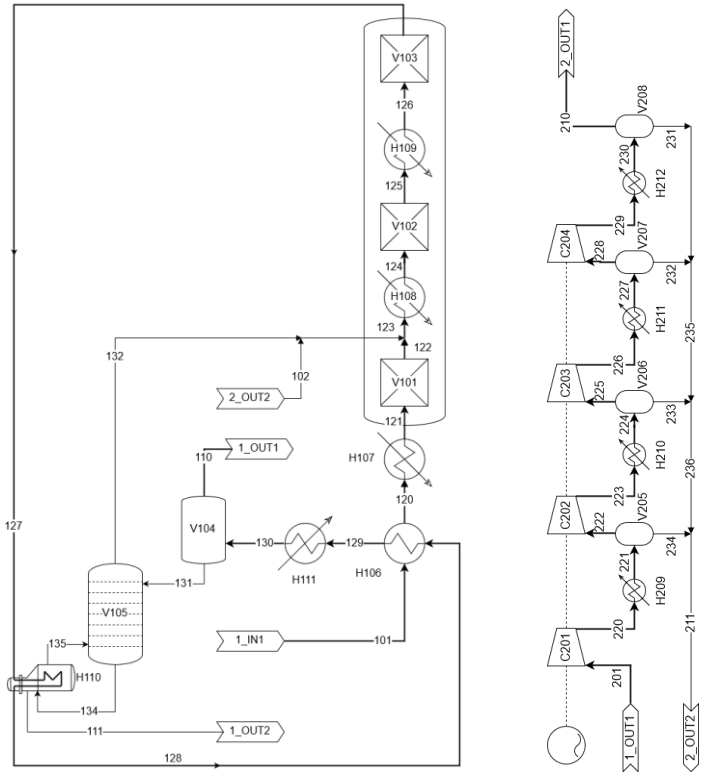

Figure 6: Ethylene reactor with water condensation and ethanol recovery (left), and compression with further water separation (right).

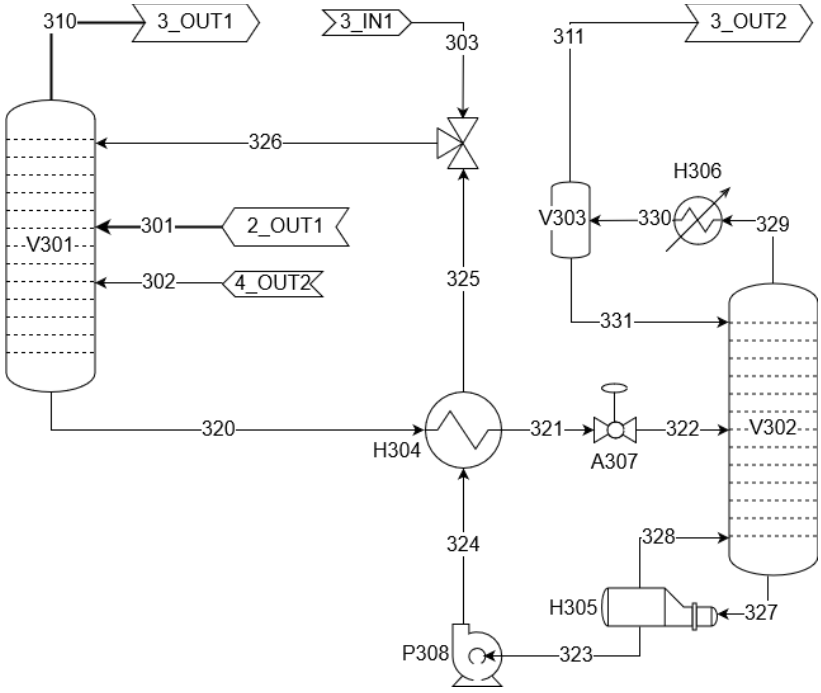

Figure 7: CO_2 absorber and stripper for amine-base washing.

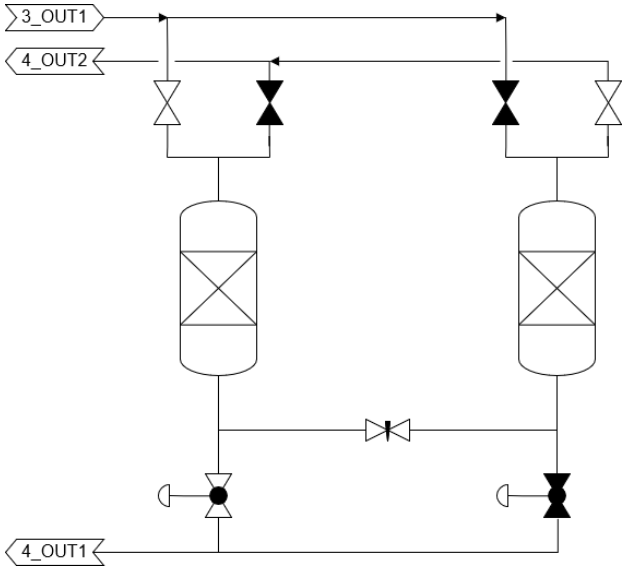

Figure 8: Basic scheme of a two-bed PSA system.

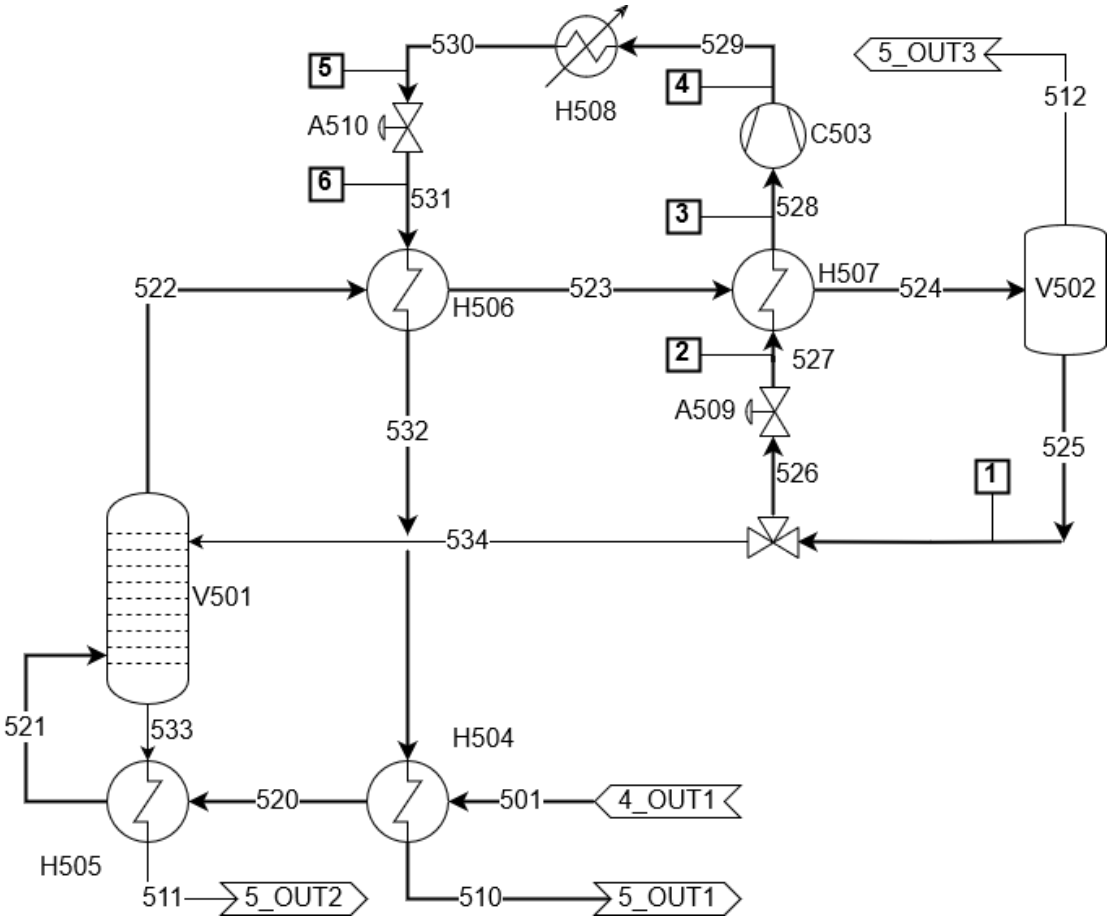

Figure 9: Diagram of the ethylene tray-column with partial condenser and refrigeration blocks. Numbers in the squares are referred to the process in **Figure 20**.

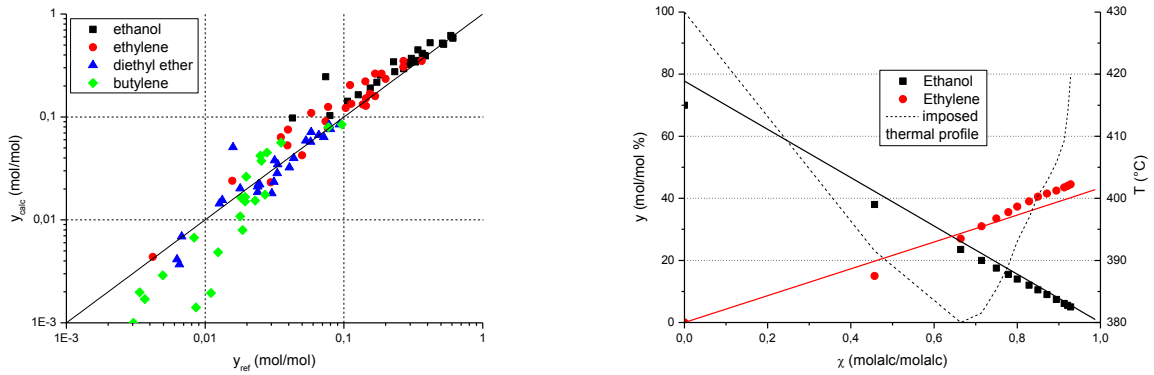

Figure 10: Test of the adopted kinetic model to reproduce the original data of [49] (left), and the reactor's output already calculated in [50] on the basis of the same data (right).

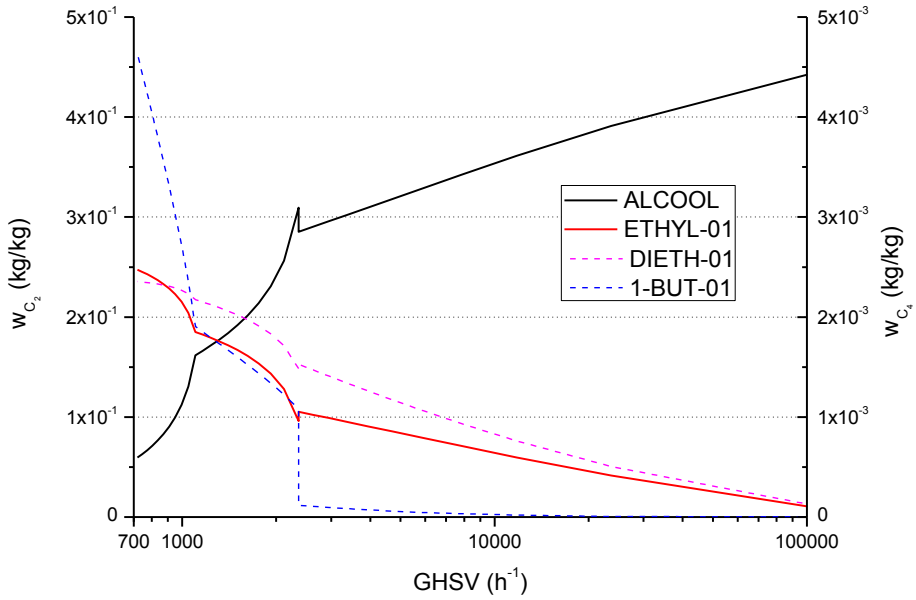

Figure 11: Molar concentration of the main species within the reactor as a function of GHSV. The kink (or step) marks the recycle inlet point after the first stage.

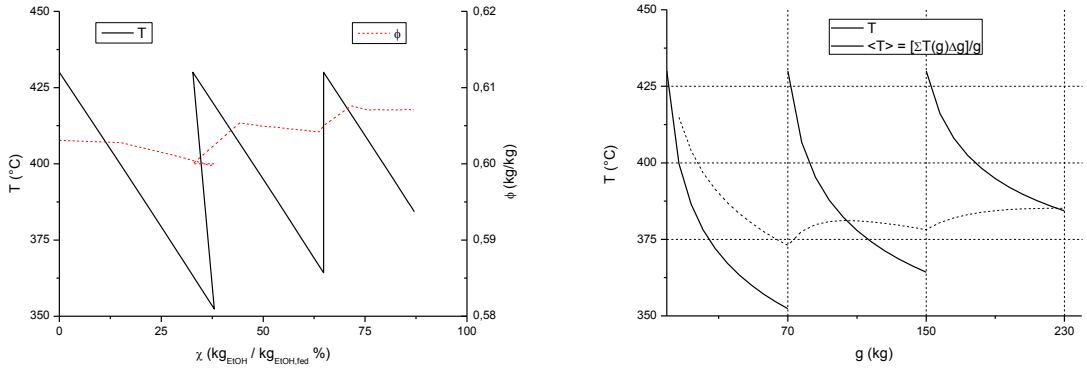

Figure 12: Thermal profile as a function of ethanol conversion (left) and catalyst load (right).

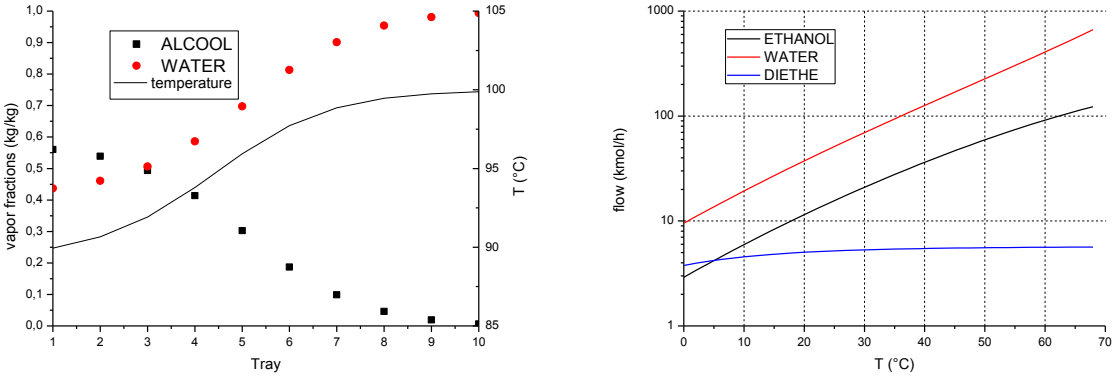

Figure 13: Composition of the vaporized recycled stream along the recovery column (left) and variation of the vapor flows at the first separator according to temperature.

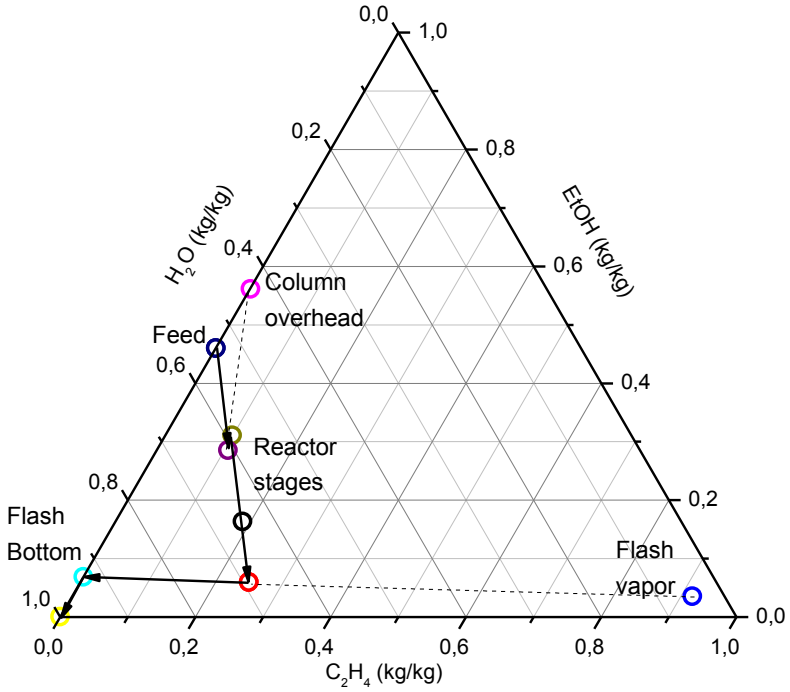

Figure 14: General evolution of the process stream through the first process units.

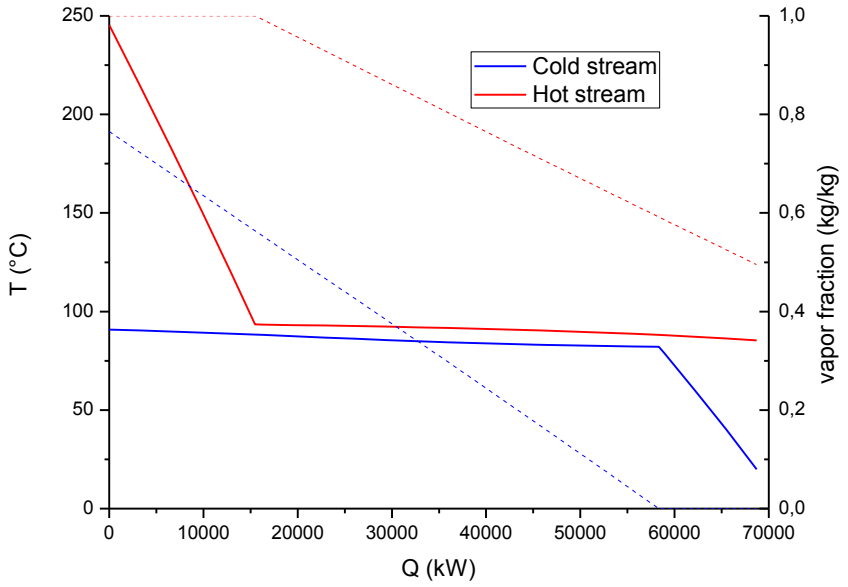

Figure 15: Thermal profiles of the feed-to-product heat exchanger.

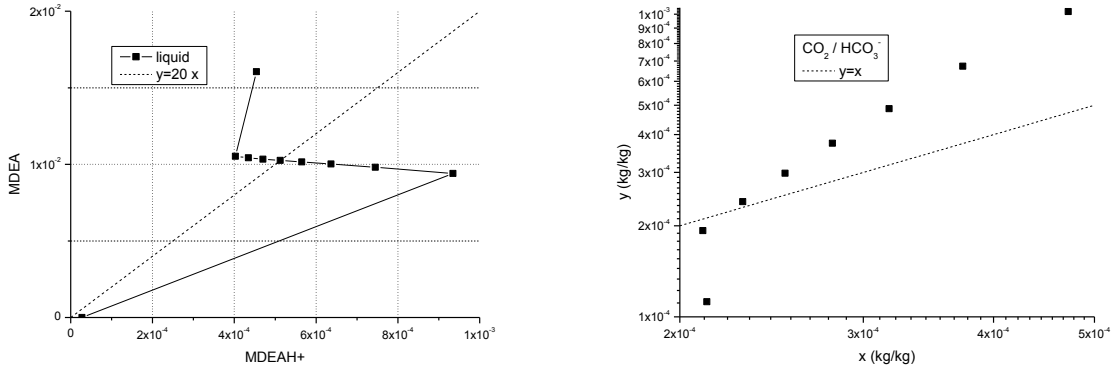

Figure 16: Relation between the main neutral and charged species along the trays of the CO_2 stripper.

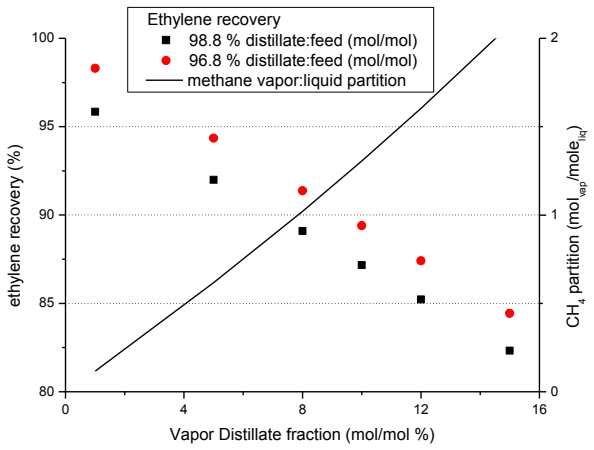

Figure 17: Behavior of the partial condenser of the ethylene purification column as a function of the vapor/liquid distillate ratio for 2 different ethylene recoveries.

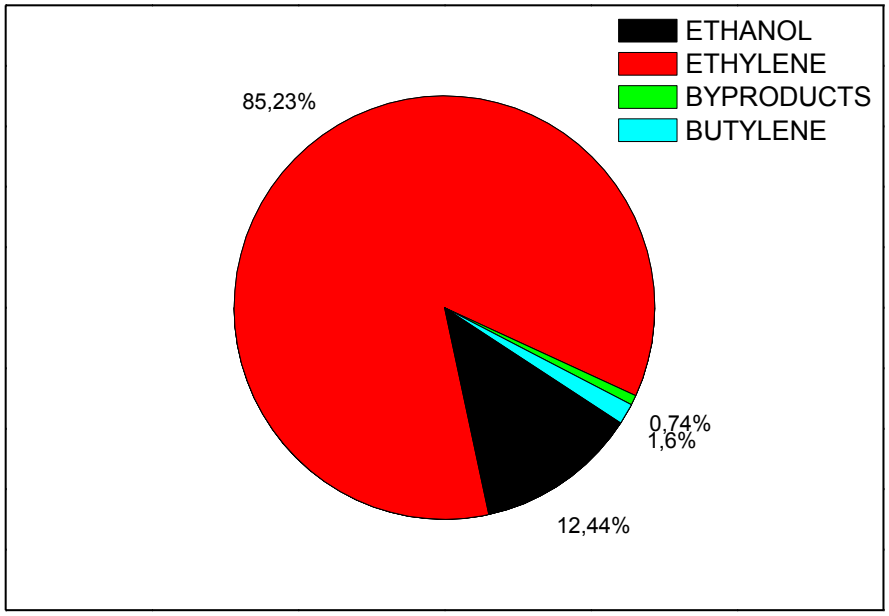

Figure 18: Carbon atom distribution after the reactor, before the ethanol recycles.

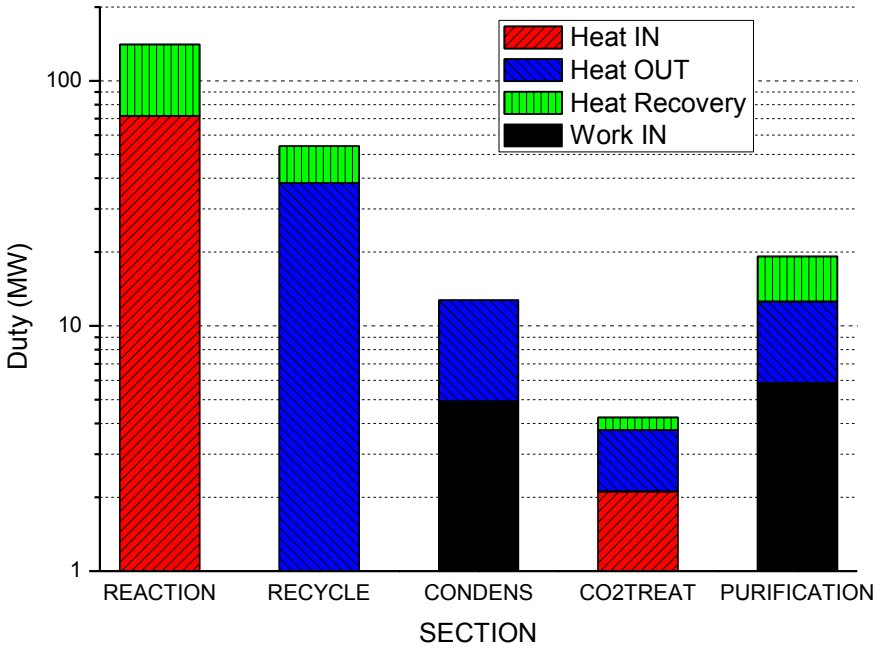

Figure 19: Gross energy balances of the plant sections. The work and cooling duties for the recycle between sections 3-4 are not counted.

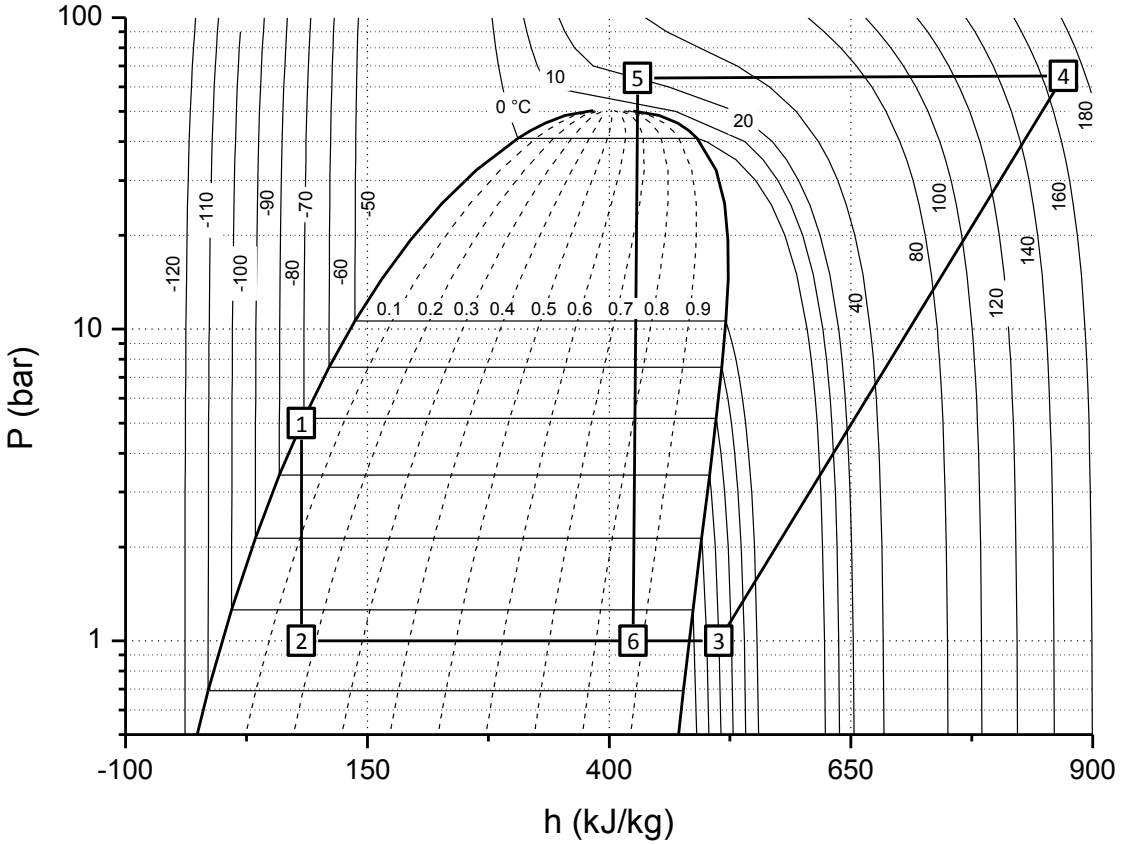

Figure 20: Ethylene pressure-enthalpy chart for a basic cryogenic cooling of plant section in **Figure 9**. The 3-4 compression follows a nearly isentropic path.

TOC

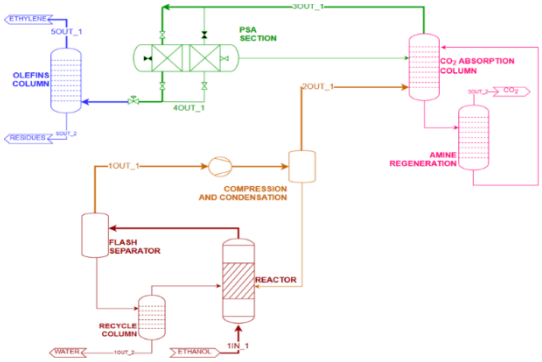

A bioethylene production plant is presented starting from renewable bioethanol. Diluted feed improves the economic sustainability and intensifies the process.